NTNU

Norwegian University of
Science and Technology

Grain Refinement of High Alloyed Steel With Cerium Addition

Eivind Strand Dahle

Materials Technology
Submission date: July 2011
Supervisor: Øystein Grong, IMTE

Norwegian University of Science and Technology
Department of Materials Science and Engineering

Preface

The following work has been carried out at the Department of Materials Technology, Norwegian University of Science and Technology (NTNU) from February to July 2011. The work has been in collaboration between NTNU, Elkem, Sintef and Scana Steel Stavanger.

Professor Øystein Grong have been the supervisor, along with Dr.ing. Casper van der Eijk (SINTEF), Dr.ing. Ole Svein Klevan(Elkem) and Dr. Fredrik Haakonsen (SINTEF) as co-supervisors.

I would also like to thank Yingda Yu for help with the SEM examination, and Morten Raanes for executing the EPMA examination.

Trondheim

July 2011

Eivind Strand Dahle

Abstract

This master thesis has the objective to improve the mechanical properties of Super Duplex steel by adding Elkem Grain Refiner (EGR). EGR is commercial grain refiner where the active element is cerium. Cerium is a strong oxide and sulphide former whose inclusions are to act as sites for heterogeneous nucleation during casting. The cerium inclusions will form at low undercooling making it possible to grow equiaxed grains ahead of the solidifying front, reducing the size of the columnar zone normally seen in an ingot. By reducing the columnar zone the steel will have a larger zone of equiaxed, and smaller, grains improving the mechanical properties of the steel and reducing the segregation throughout the ingot. The experiment was performed with S4501 Super Duplex steel provided by Scana Steel Stavanger. The casting was done at Frekhaug stål, Bergen by adding 0.05, 0.075 and 0.1 wt% cerium to 120 kg casts. There were a total of 3 parallels, where 1 was cast at 1525ºC and 2 series at 1540ºC. The as cast structure was significantly refined, the columnar zone was reduced from 22 mm to being absent in the cast with most cerium added. The mechanical results show a linear increase in both yield and ultimate tensile strength with increasing amount of cerium. The elongation increased somewhat, but the impact toughness decreased linearly with increasing cerium content. The casting temperature did not seem to have an effect on the grain refining.

Table of contents

1. Introduction

Steels with high chromium and high nickel contents have for years been used in demanding corrosive environments. The alloys are available in a wide variety of versions. These steels are mostly used in marine construction, chemical industries and power plants due to the combination of mechanical properties, corrosion resistance and availability.

Duplex stainless steels contain roughly 18-26% Cr, 3-8% Ni as the main alloying elements, causing the steel to have both a ferritic and austenitic microstructure. The first commercial product was available as early as 1929, however most of the development happened since the 1970s, due to the advances in refining. [1]. The super duplex alloys came in the 1980s, with slightly higher alloy content, giving the steels a PRE_N value of at least 40, which separates super duplex from duplex.

Compared to fully ferritic or austenitic stainless steel, duplex steel combines the mechanical properties of the two. Increased ferrite content in austenitic steel increases its strength and weldability, but reduces the toughness and elongation. Typical strength for a cast duplex steel is 500 MPa yield, 750 MPa ultimate tensile strength. The goal for this report is to increase these values by refining the microstructure by adding cerium in to the melt.

Duplex steel solidifies completely as δ-ferrite, followed by solid state transformation to ~50 vol% austenite during cooling. This formation will not change the grain size as low alloyed steel, any grain refinement must therefore happen during solidification. A cast ingot can usually be separated into 3 different zones; chill, columnar and equiaxed zone. The chill zone will be small equiaxed grains located along the mould wall where solidification is quick, but when the cooling rate decreases the grains will grow as columns into the ingot. After the columnar growth there will be equiaxed grains in the centre. An ingot with a large columnar zone will have large segregations compared with a small or none columnar zone. The size of the columnar zone is therefore important regarding the mechanical properties of the ingot.[2]

To improve the mechanical properties, particles can be introduced to act as impurities for nucleation of equiaxed grains ahead of the solidifying front. For nucleation ahead of the columnar zone to occur, an undercooled region is required for precipitation of such particles. Such an undercooling can be achieved when dendrites grow into the melt, pure metal will solidify first and push solute ahead of the dendrite tip causing the liquid in front of the dendrite contain higher solute than the rest of the liquid, thus lowering the liquidus temperature causing a constitutional supercooling. When stable particles form ahead of the columnar zone new grain can nucleate much like solidification against the mould wall. A high number of such nucleation sites can make an ingot consist completely of equiaxed grains reducing segregation and improving the mechanical properties.[3]

Cerium based particles have in recent years been tested as nucleation sites for heterogeneous nucleation for austenitic and duplex steels. The results show a correlation between reduced columnar zones with added cerium [4][sintefrapport]. Cerium particles have shown promising properties regarding nucleation in steel due to requiring low undercooling for precipitation of cerium sulphides and oxides and the degree of atomic misfit is low. Elkem have in recent years, in cooperation with Sintef, developed grain refiners containing cerium. Elkem Grain Refiner (EGR) is an alloy containing ~10% cerium along with elements present in the liquid. The grain refiner is added to the tap stream before casting of the component, making cerium react with impurities as sulphur and oxygen to precipitate particles.

Scana Steel Stavanger have previously used EGR with super duplex steel after experienced increased forgeability, but have had problems with large oxide inclusions with detrimental effect of the products. Therefore Scana Steel wishes to explore the possibility to add EGR to super duplex without these problems.[5]

The experiments described in this report were done at Frekhaug stål, with steel supplied by Scana Steel Stavanger. The experiment consisted of adding EGR to super duplex steel supplied by Scana Steel in various

amounts to 3 parallels. Test blocks were designed to provoke typical ingot solidification, giving a structure with chill, columnar and equiaxed zone. The blocks were later examined by macro/microscopy, mechanical testing and SEM/EPMA.

2. Theoretical background

2.1 Structural zones in casting

Generally a casted ingot will have three different zones. Near the mould wall there will be an outer chill zone of equiaxed crystals, a columnar zone of elongated grains, and an equiaxed zone in the centre. Often one of the zones is missing; in stainless steels the structure can be fully columnar, with no central equiaxed zone and no chill zone. A well grain refined aluminium alloy can have a structure of completely equiaxed grains. The occurrence and degree of these zones are known to depend both on nucleation and on crystal multiplication. [2]

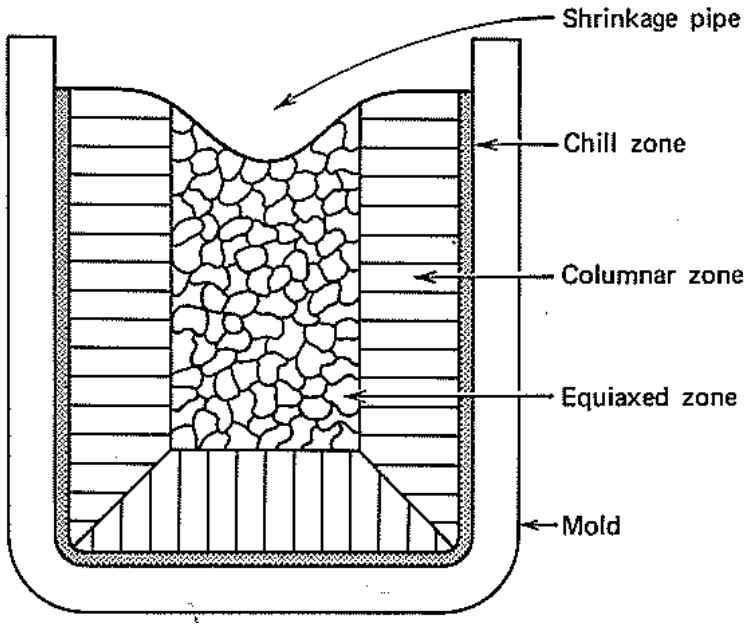

Figure 2.1: The different zones in a cast ingot.[6]

2.1.1 Chill zone.

During casting the liquid metal comes in contact with the cold and is rapidly cooled below its liquidus temperature. The undercooling will cause the liquid to form many solid nuclei along the mould wall which will grow into the liquid, some grains more than others. [3]

2.1.2 Columnar zone.

Soon after pouring the temperature gradient of the liquid near the mould wall decreases and the crystals in the chill zone grow dendritically in certain crystallographic directions, <100> for cubic metals. Crystals with the <100> directions parallel to the largest temperature gradient, perpendicular to the mould wall, will outgrow neighbours with a less favourable direction. This leads to the formation of the columnar zone, all with nearly the same orientation. The diameter of the grains can increase making it possible for some ternary arms to grow ahead of their neighbours and becoming new primary arms as shown in the figure. This is simply due to a corresponding decrease in the cooling rate with time after pouring. The region between the tips of the dendrites and the point where the last drop of liquid is solidifying is known as the mushy or pasty zone. The length of this zone depends on the temperature gradient and the non-equilibrium freezing range of the alloy.[3]

2.1.3 Equiaxed zone

The centre of an ingot often consists of equiaxed grains randomly oriented. One origin of these grains is thought to be remelted dendrite side arms, called grain multiplication. The side arms are narrower at the roots, which makes it possible to isolate the arms if the temperature increases after the arm is formed. The detached arm can then act as a seed for a new crystal. Convection currents can transport the detached arm to develop into an equiaxed grain. Equiaxed grains can also grow from nucleation sites in the liquid ahead of the columnar zone. Similar to the chill zone, the grains need a solid wall to grow from, where stable particles already formed in constitutionally supercooled liquid can act as nucleation sites for new grains.[3] Equiaxed grains are beneficial in regards of mechanical properties of a metal. Seeing as the orientation will change when moving from one grain to another across a grain boundary, there is a region of disturbed lattice only a few atomic diameters thick. High angle grain boundaries have high surface energy, causing boundaries to be a source for solid-state reactions as diffusion, phase transformation and precipitation reactions. This also means a higher concentration of solute atoms than in centre of grains. When a polycrystal is under strain, the grains will try to deform homogeneously while still keeping the

boundaries intact will cause differences in the deformation between neighbouring grains and within grains. If the strain increases and grain size decreases the deformation becomes more homogeneous. Deformation bands will be created due to lattice rotations because of different slip systems in the same grain. More slip systems are in effect near the grain boundary, therefore a reduced grain size will make the effect of grain boundaries influence the centre of a grain making the metal stronger. A general relationship between yield stress and grain size is known as the Hall-Petch relation given in equation 1 [7]

$$\sigma_0 = \sigma_i + kD^{-1/2} \quad (1)$$

Where σ_0 is the yield stress, σ_i is friction stress, k is the locking parameter, and D is grain diameter.

2.2 Effect of grain refinement

2.2.1 Homogeneous nucleation

For an impurity-free liquid to solidify it requires significant cooling below its melting temperature for the driving force to be big enough to solidify the melt. If a liquid at a temperature ΔT below T_m with a free energy G_1 the atoms will cluster together to form a small sphere of solid, the free energy will change to G_2 given by:

$$G_2 = V_S G_v^S + V_L G_v^L + A_{SL}\gamma_{SL} \quad (2)$$

Where V_S is the volume of the solid sphere, V_L the volume of liquid, A_{SL} is the area of the solid/liquid interface, G^S_V and G^L_V are the free energies per unit volume of solid and liquid respectively, and γ_{SL} the solid/liquid interfacial free energy. Below T_m, G_v is positive since the free energy change with formation of a solid has a negative contribution due to lower free energy of a bulk solid, but the creation of a solid/liquid interface is a positive contribution. This gives a sphere with radius r with a free energy:

$$\Delta G_{hom} = -\frac{4}{3}\pi r^3 \Delta G_v + 4\pi r^2 \gamma_{SL} \quad (3)$$

This equation shows a dependency of r, the second term is dominant at first, but as r increases the first term will cause the product to be negative. There will be a critical r^* which is when ΔG_{hom} is at a maximum. If $r < r^*$ the free energy can be reduced by dissolution of the solid, but if $r > r^*$ the system can reduces if the solid grows, which will is referred to as a nuclei. [3]

2.2.2 Heterogeneous nucleation

For nucleation to occur at small undercooling, the interfacial energy term must be reduced. The easiest way to achieve this is to have the nucleus form in contact with either a particle or the mould wall. Assuming the solid/liquid interfacial free energy, γ_{SL} is isotropic it can be shown that for a given volume of the solid the total interfacial energy of the system is minimized if the shape of a spherical cal with a "wetting" angle θ given by the condition that the interfacial tensions γ_{ML}, γ_{SM} and γ_{SL} balance in the plane of the mould. [3]

$$cos\,\theta = \frac{(\gamma_{ML} - \gamma_{SM})}{\gamma_{SL}} \qquad (4)$$

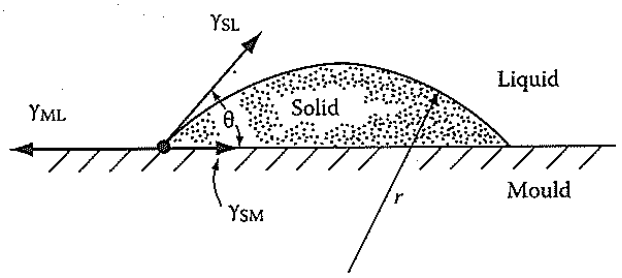

Figure 2.2: Illustration of nucleation from a solid wall.[3]

The vertical component of γ_{SL} unbalanced, forcing the mould surface upwards, giving equation (4) to define the optimum embryo shape when the mould wall remain planar. The formation of an embryo is associated with the excess free energy, which can be written in terms of the wetting angle and cap radius.

$$\Delta G_{het} = \left(-\frac{4}{3}\pi r^3 \Delta G_v + 4\pi r^2 \gamma_{SL}\right) S(\theta \quad (5)$$

Where

$$S(\theta) = \frac{(2+cos\,(\theta)(1-cos\,(\theta)^2}{4} \quad (6)$$

The expression of ΔG_{het} is the same as for ΔG_{hom} except for the $S(\theta)$ factor. This factor is only dependent on the wetting angle.

$$\Delta G_{het} = S(\theta) * \Delta G_{hom} \quad (7)$$

This expression shows a lower activation energy barrier against heterogeneous nucleation than homogenous due to the shape factor. By differentiation of equation (5) it can be shown that

$$r^* = \frac{2\gamma_{SL}}{\Delta G_v} \quad (8)$$

Which shows the critical nucleus radius being unaffected by the mould wall but and only dependent on undercooling.

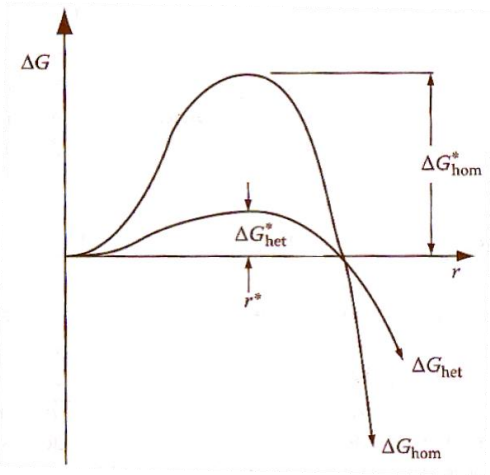

Figure 2.3: Schematic illustration of excess free energy for homogeneous and heterogeneous nucleation compared.[3]

2.2.3 Constitutional supercooling

After the first metal near the mould wall have solidified the temperature gradient will decrease rapidly. As a result of the varying solute concentration ahead of the solidification front there is also a variation in the liquidus temperature. The liquidus temperature increases with the distance from the interface because the lower the solute content the higher the liquidus temperature, illustrated in fig. 2.4. When the temperature in front of the interface is below the liquidus temperature the liquid is constitutionally supercooled, which means the supercooling comes from change in composition, not temperature. This supercooling results in instability of the plane front since any bump forming on the interface would find itself in supercooled liquid and therefore would not disappear. [2]

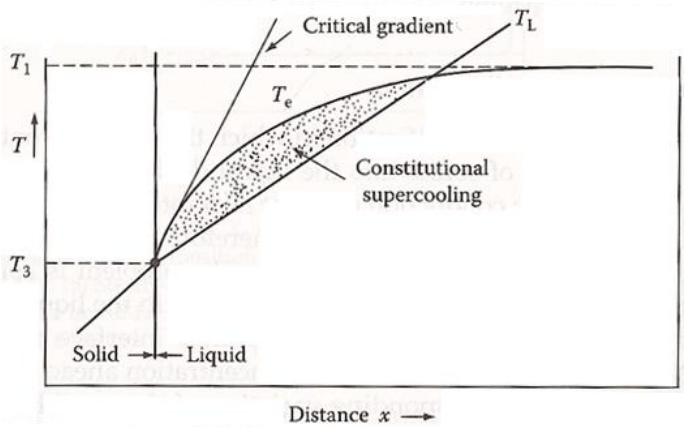

Figure 2.4: Illustration of constitutional supercooling.[3]

The concentration gradient of the liquid can be expressed

$$\frac{dc_l}{dz} = -\frac{v}{D_E} c_l(1-k) \tag{9}$$

Where D_E is a turbulent diffusion coefficient and k is a constant, v is the solidification speed and c_l is the liquid concentration. The criterion for constitutional supercooling is that the slope for the liquidus temperature (dT_1/dz) is bigger than the temperature gradient (dT/dz), which gives the following expression.

$$\frac{vb(1-k)c_b}{D_E} > \left(\frac{dT}{dz}\right)_{z=0} \quad (10)$$

This expression shows that a high solidification velocity is beneficial for the supercooling, but also a low as possible temperature gradient will increase the supercooled area. The temperature gradient can be lowered by reducing the pouring temperature.[8]

2.2.4 Cellular dendritic growth

If the temperature gradient ahead of an initially planar interface is gradually reduced below the critical value the first stage breaking down the planar interface. The formation of the first protrusion causes solute to be rejected laterally and pile up at the root of the protrusion. This lowers the liquidus temperature causing which trigger the formation of other protrusions. Assuming a region of constitutionally supercooled liquid in front of the solidifying interface, the temperature of the tip of a protrusion will be higher than the surrounding interface. Provided that the tip remains below the local liquidus temperature solidification is still possible and the protrusion can develop. But if the temperature gradient ahead of the interface is steeper than the critical gradient the tip will be raised above the liquidus temperature and the protrusion will melt again. Eventually the protrusions develop into long arms or cells growing parallel to the direction of heat flow. The solute rejected from the solidifying liquid concentrates into the cell walls which solidify at the lowest temperatures. The tips of the cells, however, grow into the hottest liquid and therefore contain the least solute. Even if the solute concentration is much smaller than maximum solubility the liquid between the cells may reach the eutectic composition in which case the cell walls will contain a second phase. Each cell has virtually the same orientation as its neighbours and together they form a single grain. [3]

Cellular microstructures are only stable for a certain range of temperature gradients. At sufficiently low temperature gradients the cells, are observed to develop secondary arms, and at still lower temperature gradients tertiary arms develop, i.e. dendrites form. Associated with this change in morphology there is a change in the direction of the primary arms away from the direction of heat flow into the crystallographically

preferred directions such as (100) for cubic metals. In general, the trend to form dendrites increases as the solidification range increases. Therefore the effectiveness of different solutes can vary widely. The reason for the change from cells to dendrites is not fully understood. However it is probably associated with the creation with the creation of constitutional supercooling in the liquid between the cells causing interface instabilities in the transverse direction. Note that for unidirectional solidification there is approximately no temperature gradient perpendicular to the growth direction. The cell or dendrite arm spacing developing is probably that which reduces the constitutional supercooling in the intervening liquid to a very low level. This would be consistent with the observation that cell and dendrite arm spacings both decrease with increasing cooling rate: Higher cooling rates allow less time for lateral diffusion of the rejected solute and therefore require smaller cell or dendrite arm spacings to avoid constitutional supercooling.[3]

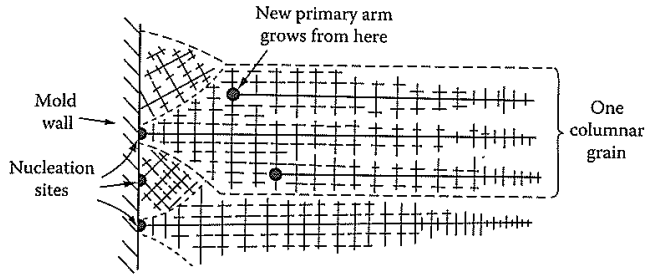

Figure 2.5: Columnar grains with similar direction of growth.[3]

2.2.5 Segregation

Two types of segregation can be distinguished in solidified structures. There is macrosegregation: composition changes over distances comparable to the size of the specimen. There is also microsegregation: segregation which occurs on the scale of secondary dendrite arm spacing. It has been known that large differences in composition can arise across the dendrites due to coring and the formation of non-equilibrium phases in the last solidifying drops of liquid. Experimentally it is found that while cooling rate affects the spacing of the dendrites it does not significantly change the amplitude of the solute concentration provided the dendrite morphology does not change and that diffusion in the solid is

negligible. The mushy zone length is proportional to the non-equilibrium solidification range, which is usually larger than the equilibrium melting range.

There are four important factors that can lead to macrosegregation in ingots: Shrinkage due to solidification and thermal contraction; density differences in the interdendritic liquid; density differences between the solid and liquid; and convection currents driven by temperature-induced density differences in the liquid. All of these factors can induce macrosegregation by causing mass flow over large distances during solidification. Interdendritic liquid flow can also be induced by gravity effects. In general segregation is undesirable as it has marked deleterious effects on mechanical properties. The effects of microsegregation can be reduced by subsequent homogenization heat treatment, but diffusion in the solid is far too slow to be able to remove macrosegregation. [3]

2.2.6 Shrinkage

Most metals shrink on solidification and this has important consequences for the final ingot structure. In alloys with a narrow freezing range the mushy zone is also narrow and as the outer shell of solid thickens the level of the remaining liquid continually decreases until finally when solidification is complete the ingot contains a deep central cavity or pipe. In alloys with a wide freezing range the mushy zone can occupy the whole of the ingot. In this case no central pipe is formed. Instead the liquid level gradually falls across the width of the ingot as liquid flows down to compensate for the shrinkage of the dendrites. However, as the interdendritic channel close up this liquid flow is inhibited so that the last pools of liquid to solidify leave small voids or pores.

2.3 Cerium as grain refiner

Cerium is a very strong oxide and sulphide former which means it that cerium will react with available oxygen and sulphur when added to liquid metal. The inclusions cerium will form are beneficial to the refine the casting microstructure by acting as sites for heterogeneous nucleation. To be a suitable nucleation site inclusion must be able to be formed at low undercooling and have a low atomic misfit with the solidifying metal.

Figure 2.7 summarizes the potential of some inclusions to act as nucleation sites for steel which solidifies as ferrite.

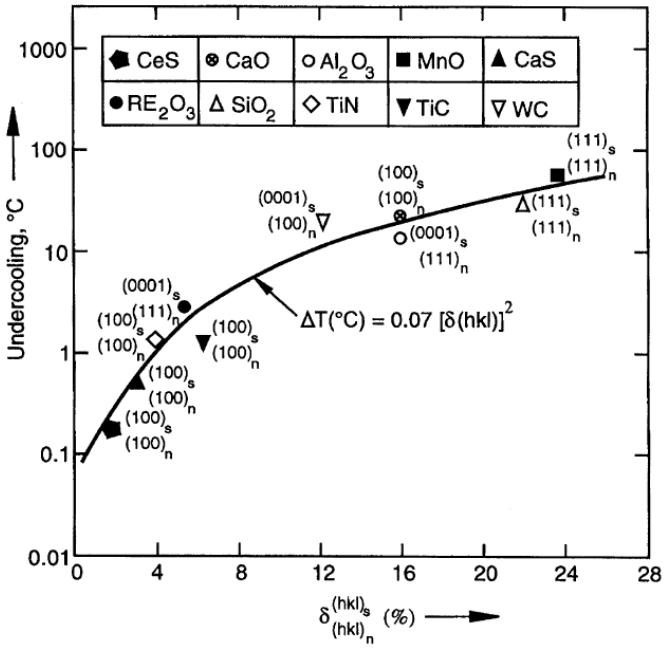

Figure 2.7 Required undercooling versus lattice misfit for different inclusions found in steel.[9]

$$\delta^{(hkl)_s}_{(hkl)_n} = \sum_{i=1}^{3} \frac{1}{3} \left(\frac{\left| \left(d_{uvw_s^i} \cos\gamma \right) - d_{uvw_s^i} \right|}{d_{uvw_s^i}} \right) \qquad (11)$$

Where $(hkl)_s$ = a low-index plane of the substrate, $[uvw]_s$ = a low-index direction in $(hkl)_s$, $(hkl)_n$ = a low-index plane in the nucleated solid, $[uvw]_n$ = a low-index direction in $(hkl)_n$, $d_{[uvw]s}$ = the interatomic spacing along $[uvw]_s$, $d_{[uvw]n}$ = the interatomic spacing along $[uvw]_n$,γ = the angle between $[uvw]_s$ and $[uvw]_n$. The degree of misfit shown in figure 2.7, and explained in equation (11) is calculated for ferrite lattice. The density of

Cerium has been used as grain refiner with success; it is often added as Elkem Grain Refiner (EGR), a master alloy consisting of Ce, Si, Cr and C. A number of experiments have used cerium as grain refiner; experiments with low alloy steel have shown a reduction of secondary

dendrite arm spacing and increase in area fraction of equaxed grains with cerium addition[10]. The columnar zone has been greatly reduced in austenitic manganese steels have and an increase in impact toughness. [4, 11, 12] Stainless steels, ferritic, austenitic and duplex, have been experimented on in regards of grain refining, where the microstructure have been refined, but not translated into improved mechanical properties.[13, 14] There have however been problems with large cerium oxide clusters during industry scale production; clusters have caused failure in components.

2.4 Inclusions in a metal

There are generally two kinds of non-metallic inclusions in steel; trapped unintentionally, or those separated from the metal due to temperature or composition change. The inclusions trapped unintentionally are normally obstructed in the melt before casting, like slag. The other inclusions are formed by reactions in the melt or precipitated when solubility decreases during cooling, normally; oxides, sulphides or nitrides. During refining the goal is to reduce the amount of these elements, but they will always be present in some amount. These inclusions can be damaging to the properties of steel. Investigation of low alloyed steel has shown that the amount of inclusions has little or no effect on ultimate tensile strength, and also a small increase in yield strength. The toughness and fatigue properties of steel have been reported to decrease, but the overall conclusion is that the type is more important than the number of inclusion.[15] Therefore process control is more important; avoiding large clusters of inclusions will determine the success of particles introduced as grain refiner.

There are a number of methods for removing unwanted inclusions; settling, flotation, filtration and stirring are the most used. In an induction furnace and a ladle without possibility for bubbling, settling is the only method available. Inclusions are often lighter than the metal, making gravity a help for removing inclusions. Light inclusions will float up to the slag, and heavier inclusions will settle to the bottom. The driving force for settling is the difference of density between the inclusion and liquid metal expressed in equation (12)

$$F_g = \Delta\rho g V \tag{12}$$

Where F_g is the gravity force, g is the gravity acceleration, $\Delta\rho$ is the difference of density and V is the volume of the inclusion. The effectiveness of the settling is determined by the relative speed of the inclusion relative to the liquid which can be expressed by equation 2.X.

$$u_r^2 = \frac{\Delta\rho g V}{\phi\rho A_p} \tag{13}$$

Where u_r is the relative speed, ϕ is an empirical friction factor and A_p is the area of the cross-section transverse to the direction of flow. The friction factor for a sphere is 12/Re. Inclusions are normally so small that that Re < 2 giving the following equation for spherical particles, known as Stoke's law:

$$u_r = \frac{2\Delta\rho g a^2}{\rho\nu 9} \tag{14}$$

Where a is the radius of the particle and v is the kinematic viscosity of the liquid. The equation is valid for particles with a radius up to 50 µm, which covers most inclusions, if the difference in density is not too big. The mixing of the inclusions in the melt is important since inclusions can, besides nucleation solidification, also influence the mechanical properties in a negative manner. The holding time is important to let the settling affect the inclusions in the, but also a too long holding time can make the cerium inclusion grow, to potentially be mechanically dangerous. A small scale experiment have found that a holding time of 5 minutes produces the most amount of inclusions, and a longer time will cause the size of the inclusions to increase.[16]

2.5 Super Duplex steel

Cast stainless steels are high alloyed steel with superior corrosion resistance in tough environments due to high contents of chromium and nickel, also nitrogen molybdenum, copper, silicon and tungsten is present to control properties. Duplex stainless steels got their name from having a mix of austenite (fcc) and ferrite (bcc) microstructure, the amount of each phase is a function of composition and heat treatment. Equal amounts of

ferrite and austenite is usually the desired ratio in these steels. Super Duplex is defined to have the pitting resistance equivalent number (PRE_N) above 40, unlike duplex steel. A high PRE_N number is crucial in high chloride environments, the equation for calculating PRE_N is given in eq. (15).

$$PRE_N = \%Cr + 3.3(\%Mo) + 16(\%N) \quad (15)$$

2.3.1 Composition and properties

The amount of the different elements determine the amount of each phase, the Super Duplex alloy used in these experiments are a Scana Steel Stavanger alloy similar to ASTM A182 F55 but with smaller range in composition than the standard. The composition of ASTM A182 F55 is given in table 2.X along the phase each element promotes. Controlling the amount of each phase is important to achieve the desired properties; both phases have some wanted and unwanted assets. Ferrite is beneficial to improve weldability, stress corrosion cracking and strength but have low toughness compared to the austenitic phase. The resistance to stress corrosion cracking is increased due to the ferrite pools in the austenite matrix making it harder for cracks to propagate.

Table 2.1: Composition of ASTM A182 F55 Super Duplex steel, and which phase the element promotes.

	C	Cr	Ni	Cu	Mn	Mo	N	P	S	Si	W
Wt%	<0.03	24.0-26.0	6.0-8.0	0.5-1.0	<1.0	3.0-4.0	0.2-0.3	0.03	0.01	1.0	0.5-1.0
Prom.	Aust	Fer.	Aust	Aust	Aust	Fer.	Aust	Fer.	-	Fer.	Fer.

Chromium is added to improve the local corrosion resistance by forming a passive oxide-layer, higher chromium content than 25% is normally not beneficial because of precipitation of intermetallic phases which leads to reduced ductility, toughness and corrosion properties. Chromium, along with other elements, promotes ferrite with varying effect. The chromium equivalent indicates the effect of each element in that regard.

$$Cr_{eq} = \%Cr + \%Mo + 0.7 \times \%Nb \quad (16)$$

As seen from equations for PRE_N and Cr_{eq} molybdenum is beneficial against pitting corrosion, as well as crevice corrosion, and stabilising ferrite. Molybdenum increases pitting resistance by suppressing active sites by creating an oxy-hydroxide or molybdate ion. [1] Molybdenum content from 2 to 3% will give increased resistance against chloride-bearing environments, crevice corrosion and pitting. Molybdenum content between 3 and 4% will weaken its resistance to highly oxidizing environments but increase the resistance against halide-bearing media and reducing acids. [17]

There are a number of elements that stabilises austenite, the nickel equivalent shows which elements promotes austenite and their effect, given in equation (17)

$$Ni_{eq} = \%Ni + 35 \times \%C + 20 \times \%N + 0.25 \times \%Cu \quad (17)$$

To achieve about equal amounts of ferrite and austenite the ferrite stabilisers need to be balanced austenite stabilisers, therefore the nickel content will primarily depend on the chromium content illustrated in figure 2.X.

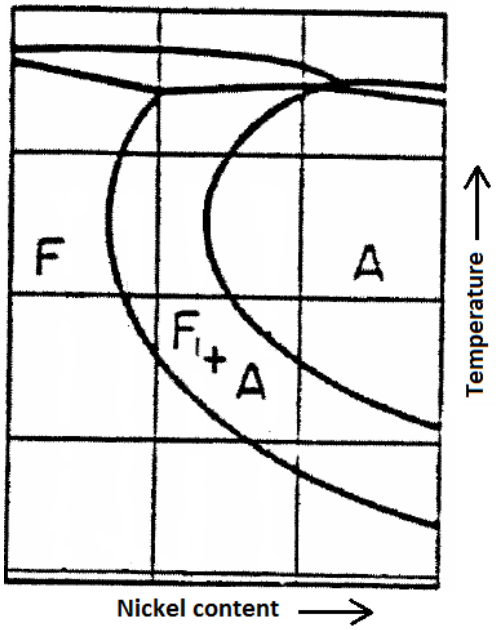

Figure 2.8: Schematic phase diagram showing increasing nickel effect on phases present, based on [18]

Too high nickel content will give austenite content above 50% which increases the chance to transform ferrite to intermetallic phases.

Carbon is present in small numbers, maximum 0.03 wt% due to the danger of chromium-carbides at grain boundaries, which is detrimental to pitting and intergranular corrosion. Nitrogen has several effects on duplex steel, even small content can increase pitting resistance, strength and austenite content as seen from eq. (15) and (17) Nitrogen has low solubility in ferrite, which solidifies first, making relative high content dangerous for pores if segregated in to the small amount of austenite present during solidification, as seen in [19]. Nitrogen content in the range 0.3-0.4 wt% will make the steel solidify as austenite-ferrite opposed to ferrite single-phase, reducing the ferrite content.[19]

There are also some elements with content below 1 wt%, manganese, copper, silicon and tungsten. Manganese, silicon and tungsten is not included in any of the equations for $PRE_N/Cr_{eq}/Ni_{eq}$, but is added for increased strength and abrasion; Mn. Crevice corrosion resistance and

pitting resistance; W. Silicon gives increased resistance to nitric acid and high temperature service, but the content is normally limited to 1 wt% due to promoting sigma phase. Cu addition is limited due to reducing hot ductility, but also reduces general corrosion.[1]

2.3.2 Heat treatment

When duplex steel solidifies, δ-ferrite dendrites are formed segregating the nickel in to austenite areas between the ferrite dendrites. This causes the steel to be heavily segregated, requiring heat treatment [19]. The first part of heat treatment is there for a homogenization to ensure a homogen steel, this is normally in the ferrite region since diffusion speed is about twice in ferrite compared to austenite. If duplex steel is cooled slowly, chromium-rich carbides form at ferrite-austenite interfaces, these carbides deplete the surrounding matrix of chromium weakening the corrosion resistance of the alloy, carbides can also lead to localized pitting. Therefore solution annealing makes the steel less vulnerable to intergranular attack. The solution annealing should also be performed at a temperature in the center of the dual phase area to give the steel equal amounts of ferrite and austenite. Figure 2.10 shows a schematic view of the phases and where homogenization and solution annealing will be done. Solution annealing is completed by water quenching.[1]

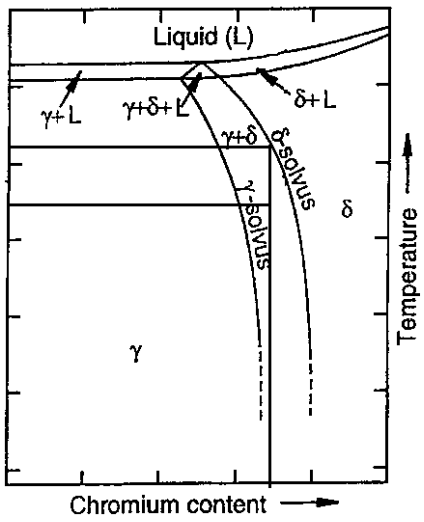

Figure 2.9: Schematic phase diagram showing typical heat treatment steps phase to homogenization and phase balance.

3. Experimental procedure

3.1 Casting

Casting of the keel blocks used in this experiment was done at Frekhaug Stål in Bergen. The blocks were cast by melting pre-alloyed blocks of S4501 Super Duplex steel supplied by Scana Steel Stavanger, S4501 is Scana own version of ASTM A182 F55. Scana Steel supplied two blocks at 790 kg each dimensioned to fit the furnace at Frekhaug. The two blocks was melted in an induction furnace, then added CaSi to deoxidise the melt. The 12 blocks which were to be cast was divided in to 3 series, each with 4 blocks where there was 1 reference and 0.05%, 0.075% and 0.1% Ce respectively added to the ladle.

Table 3.1: Overview of block cast, addition of Ce and Al and casting temperature

Block #	% Ce	% Al	Casting temp
1	-	0.021	1525°C
2	0.05	0.021	1525°C
3	0.075	0.021	1525°C
4	0.1	0.021	1525°C
5	-	0.021	1540°C
6	0.05	0.021	1540°C
7	0.075	0.021	1540°C
8	0.1	0.021	1540°C
9	-	0.021	1540°C
10	0.05	0.021	1540°C
11	0.075	0.021	1540°C
12	0.1	0.021	1540°C

The aimed casting temperature was 1540°C, but the first series of 4 blocks were cast at 1525°C to examine the effect of casting temperature. The cerium containing masteralloy (EGR) was added just after FeAl into the ladle during tapping from the furnace. Each cast consisted of 120kg liquid in the ladle. The measure the time of each cast is given in figure 3.1. The figure shows the time from start tapping from furnace, to EGR addition, tapping stop, pouring into the mould start and finish. The various lengths of time between tapping stop and pouring start was to reach the desired temperature, varying from 19 seconds in cast #1 to 2

minutes, 6 seconds for cast #11, the blocks were cast in the order shown in the figure.

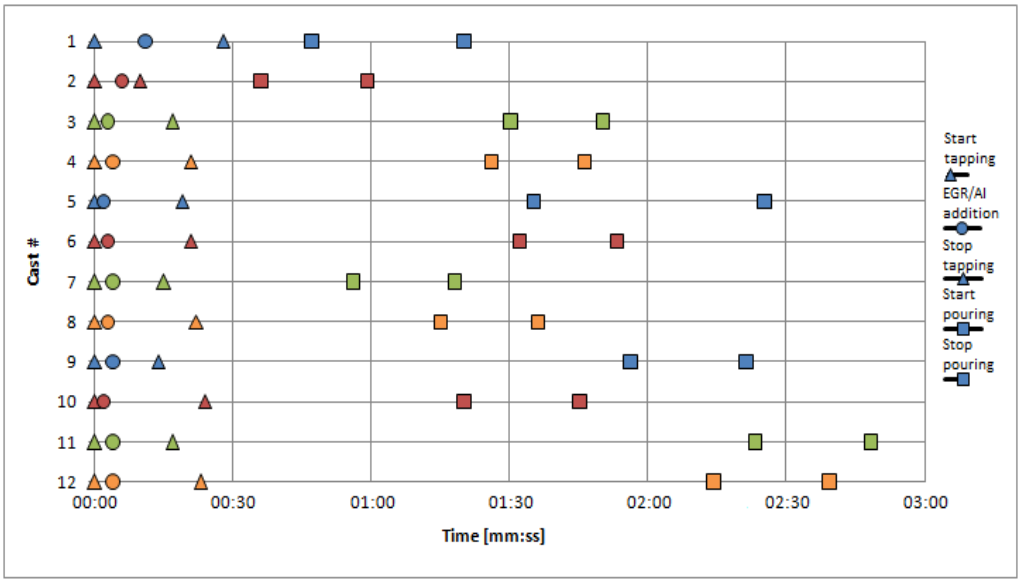

Figure 3.1: Time used for each cast from start to finish.

The moulds were made at Frekhaug Stål, had dimensions 250 x 120 x 110 mm excluding the feeder, illustrated in figure 3.2. After cooling, a part with dimensions 50 x 120 x 110 mm was cut to examine the as cast structure of the cross section of the block. The remaining part was heat treated at Frekhaug Stål. The heat treatment consisted of a homogenization treatment for 2 hours at 1130°C followed by 2.5 hours at 1070°C for phase balance followed by water quenching from this temperature to retain the phase composition and avoid sigma phase formation.

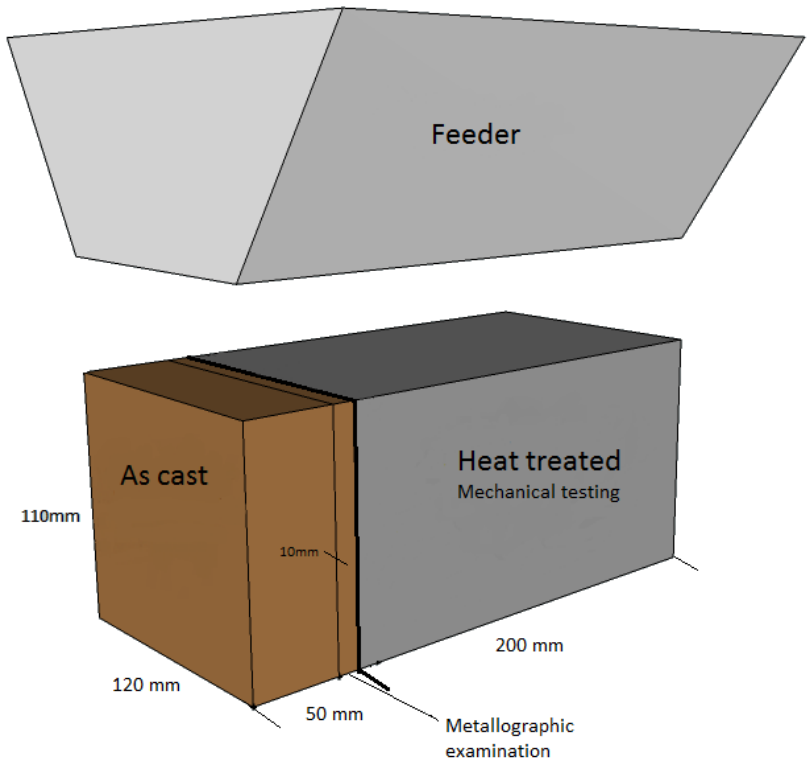

Figure 3.2: Geometry of block, showing cuts for mechanical testing and macroscopic examination.

3.2 Mechanical testing

The samples for mechanical testing were cut from 20 mm thick slice 10 mm below the feeder. The placements of the test bars are given in figures 3.4 and 3.5. From each block there was cut 2 tensile test specimens, they were cut side by side from ¼ of width of the block, farthest away from the inlet. The impact toughness specimens were cut from ¼ of width of the opposite side from the tensile specimens, cutting all 3 specimens longitudinal starting from farthest away from the inlet. The dimensions of the specimens were according to standard ASTM E23. The tensile tests were performed at room temperature, while the impact toughness tests were performed at -46°C with liquid CO_2 as cooling agent. The hardness tests were performed on the tensile bars.

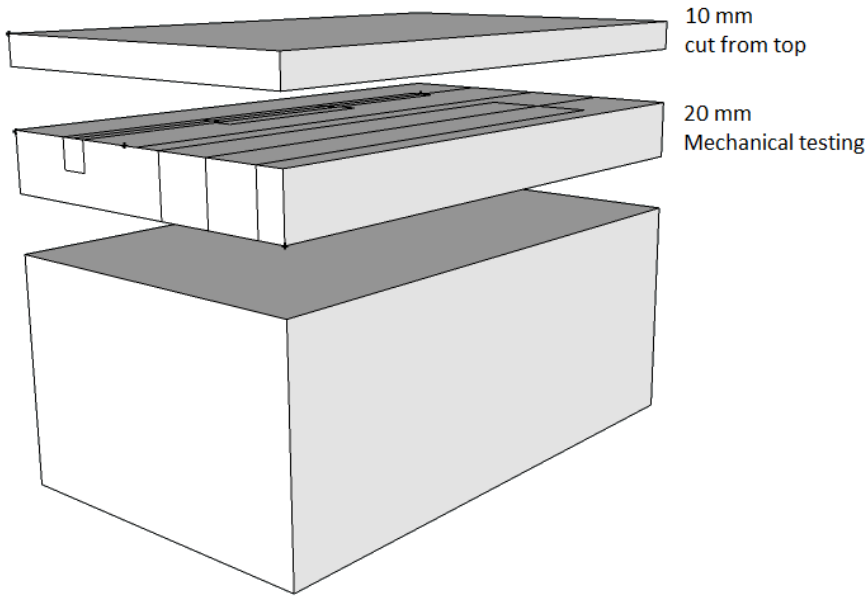

Figure 3.3 Overview of mechanical testing samples in block.

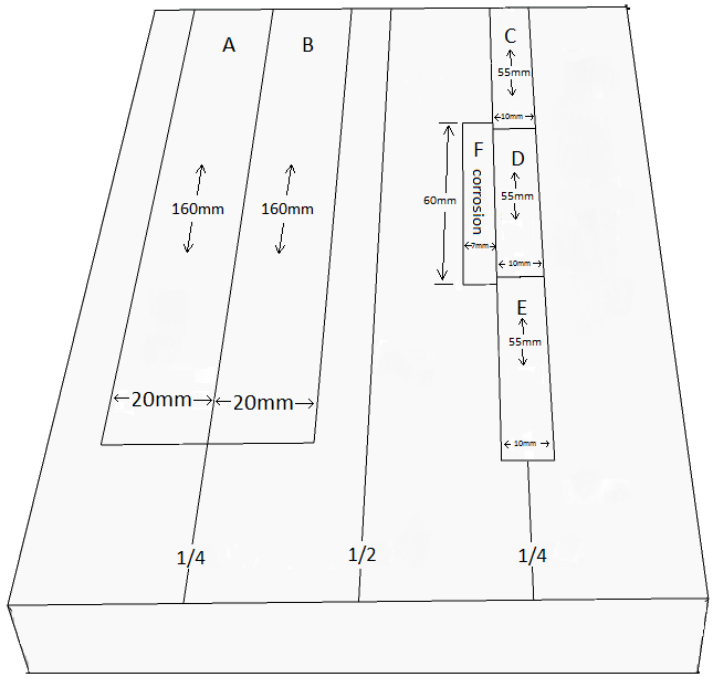

Figure 3.4 Dimensions of mechanical test samples.

3.3 Chemical analysis

The chemical analysis was performed with an optical Emission Spectrograph at Scana Steel Stavanger, every tensile bar was analysed two times, making the result for each block an average of 4 analyses. Cerium and oxygen content were analysed by combustion at D-lab, Degerfors, Sweden.

3.4 Macroscopic examination.

The keel block was cut in to two parts, one piece was kept in it's as cast condition to examine the structure. A 10 mm thick cross section was etched in concentrated HCl diluted 50-50 with distilled water. The etchant was heated and kept at 70-80°C, etching the samples for 15 minutes. The samples got a dark layer during etching which was removed by adding a few ml of concentrated HNO_3 at the end. The samples were photographed with a Canon D60.

3.5 Microscopic examination

The microscopic examination was performed on samples from charpy specimen E, which showed the most consistent results. The specimens was cut 10 mm from the fracture and cast in 25 mm diameter Struers ClaroCit. The samples were manually grinded in a Struers Knuth-rotor in mediums 80, 500 and 1200p discs, followed by polishing in a Struers DP-U3 with mediums 3 and 1 µm. The samples were etched electrolytic in 40% NaOH at 8 volt potential until visible reaction, which was after about 3 seconds. The samples were photographed with Progress C10 plus digital camera attached to a Leica MeF4M light microscope. Measuring of ferrite content was performed by software scan at Scana Steel by scanning 10 different areas of each block to determine volume amount of ferrite.

3.6 SEM/EPMA

The fracture surfaces were also examined in a Zeiss Ultra 55, the samples were kept in a desiccator to avoid contamination of the surface. The fracture surfaces were imaged with secondary electrons and visible particles in the fracture dimples were analyzed with EDS to determine if cerium was present, or other differences between the samples.

The Electron Probe Micro Analysis (EPMA) was performed on the samples used for light microscopy. Areas with a high number of particles were chosen to be pictured and subsequently identify particle composition. Particles containing cerium will be a lot brighter due to atomic number contrast, areas with bright particles were chosen deliberately. The instrument used was Jeol JXA-8500F with 5 Wavelength dispersive X-ray spectrometers.

4. Results

4.1 Chemical analysis

Chemical compositions are given in table 4.1; some elements which were present in very small amounts are not included in this table. The variation between the different casts shows that EGR did not significantly alter the balance between the elements, but the Si-content is higher in cast 7,8,11 and 12 which was added the most EGR. Traces of cerium are found in all 3 references, which is either residue from the casts added with EGR, or inaccurate analysis. There was not found any trace of Ca, which was added as CaSi to the furnace for deoxidation, but the oxygen content averaged of 430 ppm indicates unsuccessful deoxidation. The amount Si varies since it was added both as CaSi and as EGR. The references contain less Si than the blocks with EGR added, and it increases with more EGR added.

Table 4.1: Chemical composition of all blocks,

	C	Si	Mn	Cr	Mo	Ni	Al	W	N	O	Ce
1	0.029	0.370	0.540	25.0	3.65	7.22	0.006	0.585	0.261	0.035	0.007
2	0.027	0.390	0.525	24.9	3.65	7.20	0.004	0.575	0.253	0.039	0.034
3	0.028	0.380	0.533	24.9	3.65	7.21	0.005	0.580	0.257	0.042	0.036
4	0.027	0.385	0.529	24.9	3.65	7.21	0.004	0.578	0.255	0.041	0.064
5	0.027	0.360	0.480	24.8	3.68	7.29	0.004	0.570	0.258	0.040	0.009
6	0.028	0.400	0.460	24.7	3.68	7.33	0.006	0.570	0.264	0.050	0.049
7	0.028	0.430	0.530	25.1	3.65	7.23	0.006	0.570	0.253	0.043	0.052
8	0.028	0.475	0.520	25.1	3.61	7.14	0.004	0.565	0.250	0.047	0.073
9	0.028	0.345	0.510	25.0	3.67	7.29	0.004	0.575	0.254	0.034	0.006
10	0.028	0.395	0.500	25.0	3.65	7.26	0.006	0.570	0.257	0.047	0.035
11	0.028	0.430	0.480	24.9	3.63	7.16	0.007	0.570	0.252	0.051	0.067
12	0.028	0.450	0.460	24.9	3.63	7.22	0.006	0.575	0.255	0.052	0.078

The analysed cerium content is plotted versus added cerium in figure 4.1, the trend lines show average yield of the two casting temperatures; 78%

yield for 1540°C and 60% for blocks cast at 1525°C; while the overall yield is 72%.

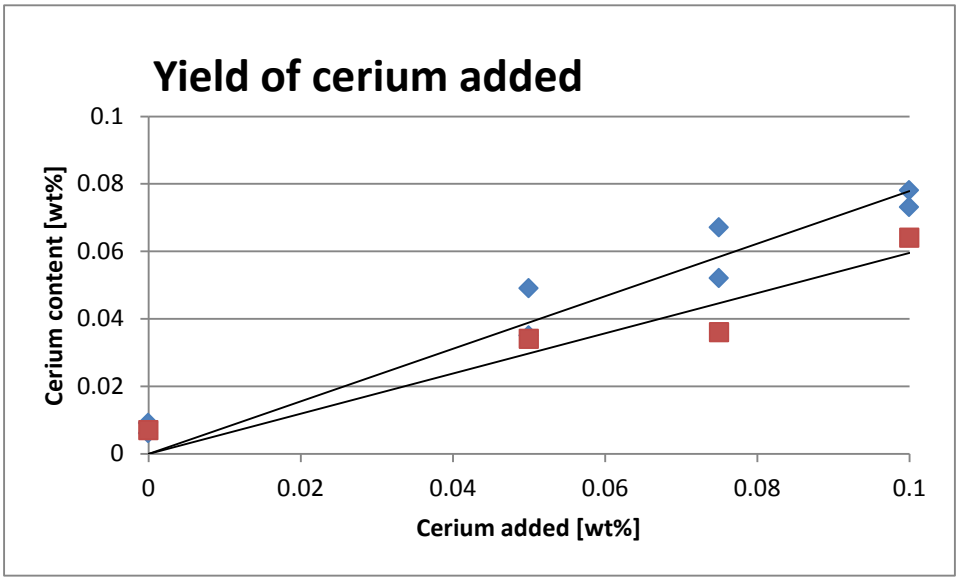

Figure 4.1: Graph of cerium analysed versus cerium added, lines showing average yield for series cast at 1540 ºC (blue) and 1525ºC (red).

4.2 Macroscopic examination

The images of the cross section of the blocks 1-4 and 9-12 in their as cast condition is shown in figures 4.2-4.9. The images clearly show reducing length of columnar zone with increasing amount of cerium, summarized in table 4.2. The images also show a smaller grain size in the equiaxed zone with increased cerium content, but this has not been quantified.

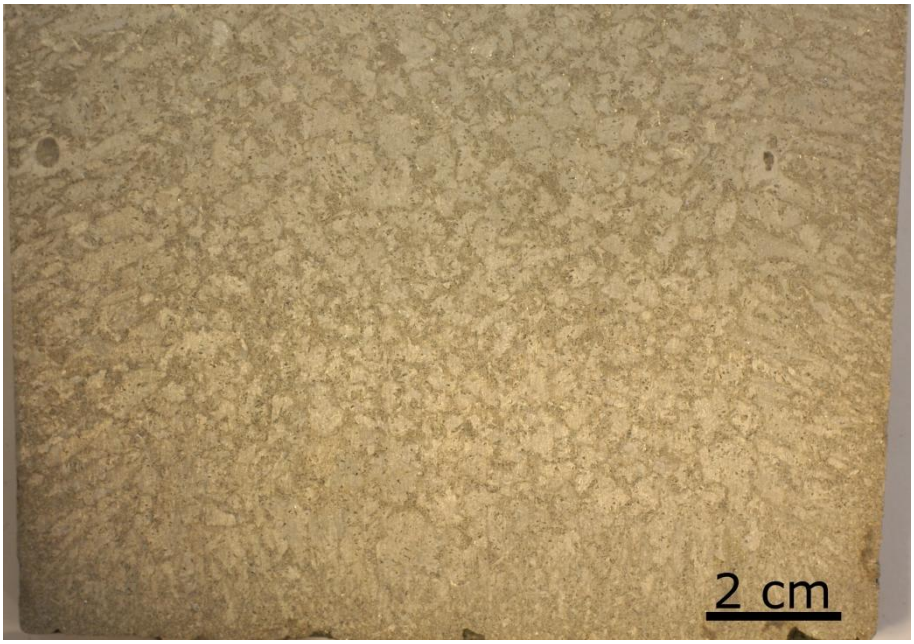

Figure 4.2: Cross section of the as cast block #1 cast at 1525°C, 0% cerium added.

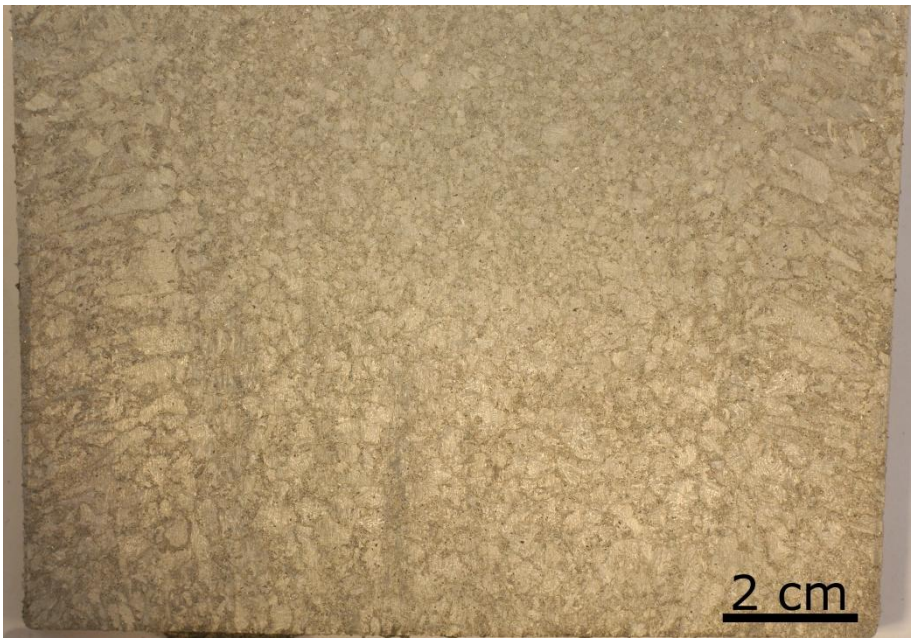

Figure 4.3: Cross section of the as cast block #2 cast at 1525°C, 0.034% cerium.

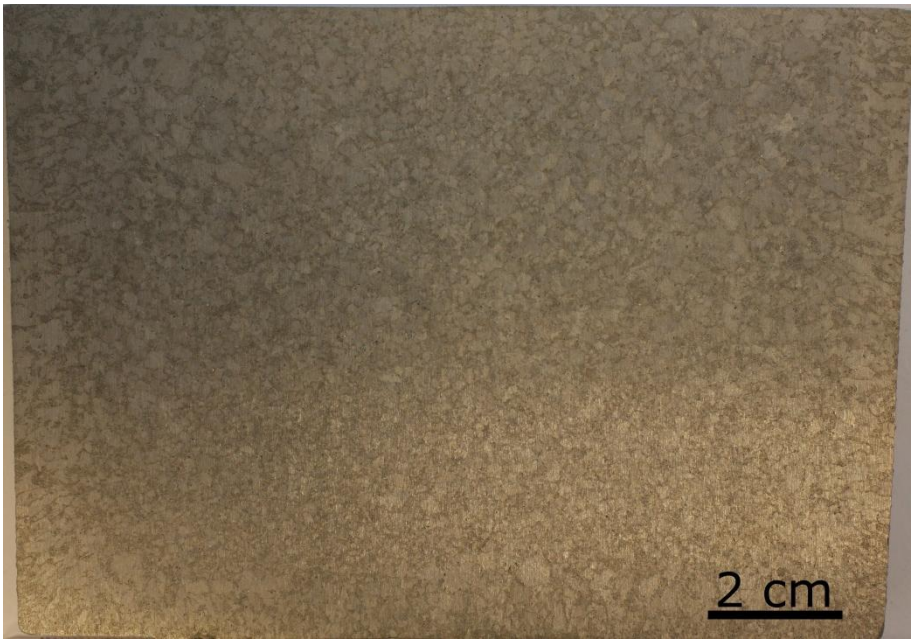

Figure 4.4: Cross section of the as cast block #3 cast at 1525°C, 0.036% cerium.

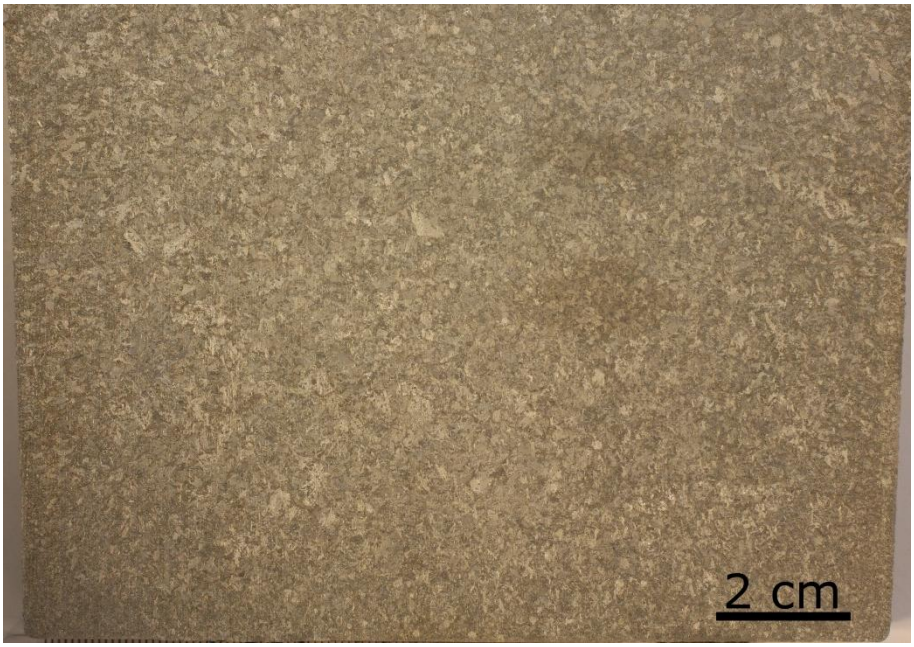

Figure 4.5: Cross section of the as cast block #4 cast at 1525°C, 0.064% cerium.

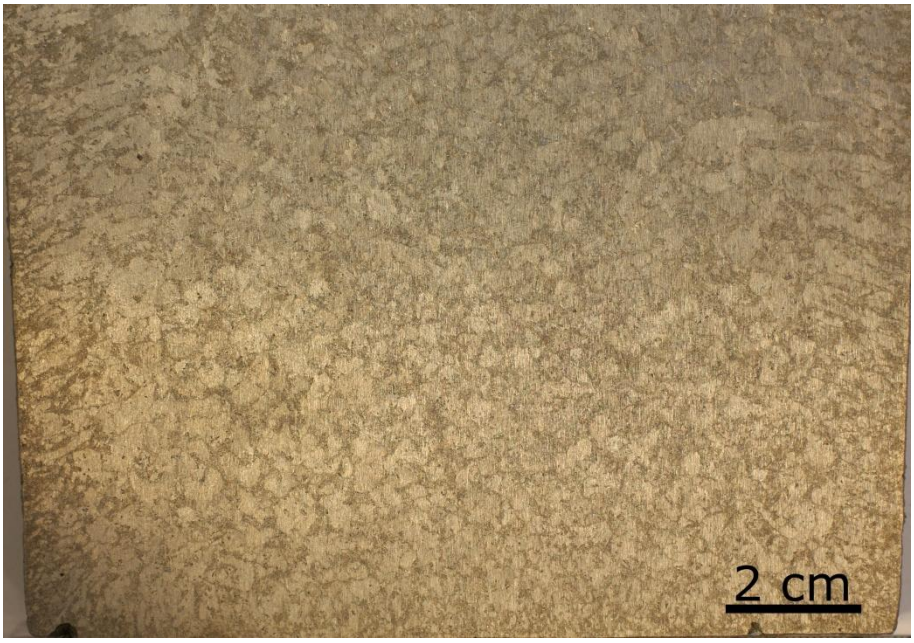

Figure 4.6: Cross section of the as cast block #9 cast at 1540°C, 0% cerium added.

Figure 4.7 Cross section of the as cast block #10 cast at 1540°C, 0.037% cerium.

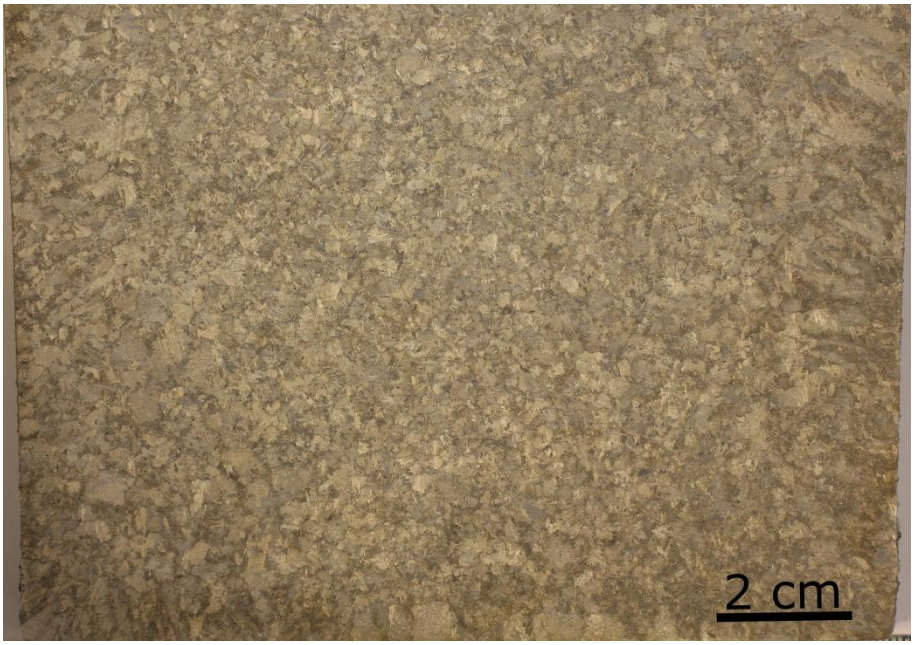

Figure 4.8: Cross section of the as cast block #11 cast at 1540°C, 0.067% cerium.

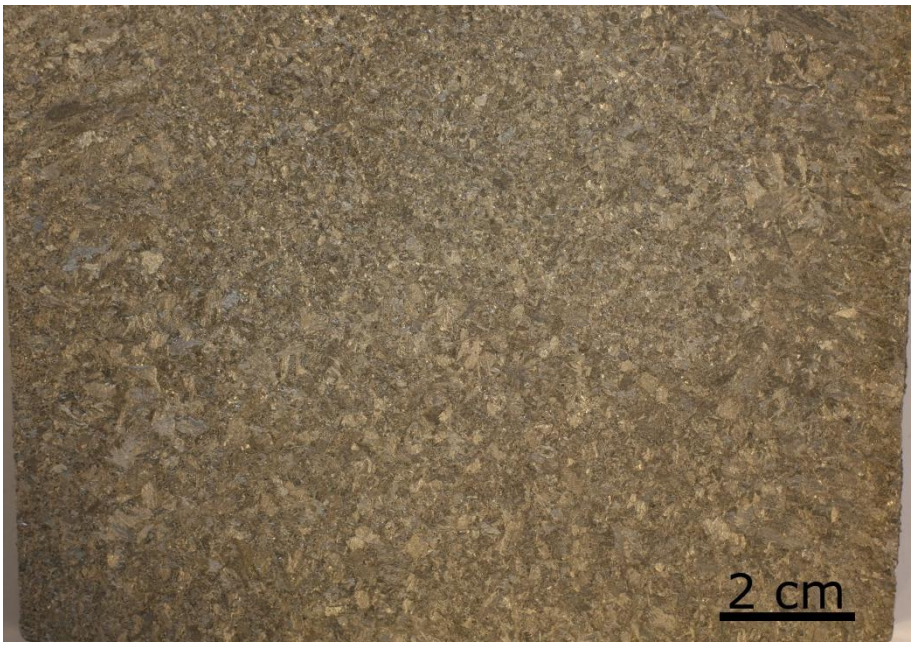

Figure 4.9: Cross section of the as cast block #12 cast at 1540°C, 0.078% cerium.

Table 4.2: Length of columnar zone with cerium content.

Block	Length of columnar zone[mm]	Cerium content [wt%]
1	22.5	0.007
2	22	0.034
3	7.5	0.036
4	0	0.064
5	23	0.009
6	18.5	0.049
7	13.5	0.052
8	0	0.073
9	19	0.006
10	19	0.035
11	16.5	0.067
12	0	0.078

4.4 Light microscopic examination

Images acquired from light microscopic examination are given in figures 4.10-4.13, the examination did not reveal much about the microstructure since it is difficult to determine grain size for the dual phase nature of the steel. Ferrite content versus cerium content is given in figure 4.14 for the blocks cast at 1540ºC, which does not show correlation between phase balance and cerium content. The ferrite content versus Ce content is plotted in figure 4.37, showing a slight increase of ferrite with increasing amount of Ce.

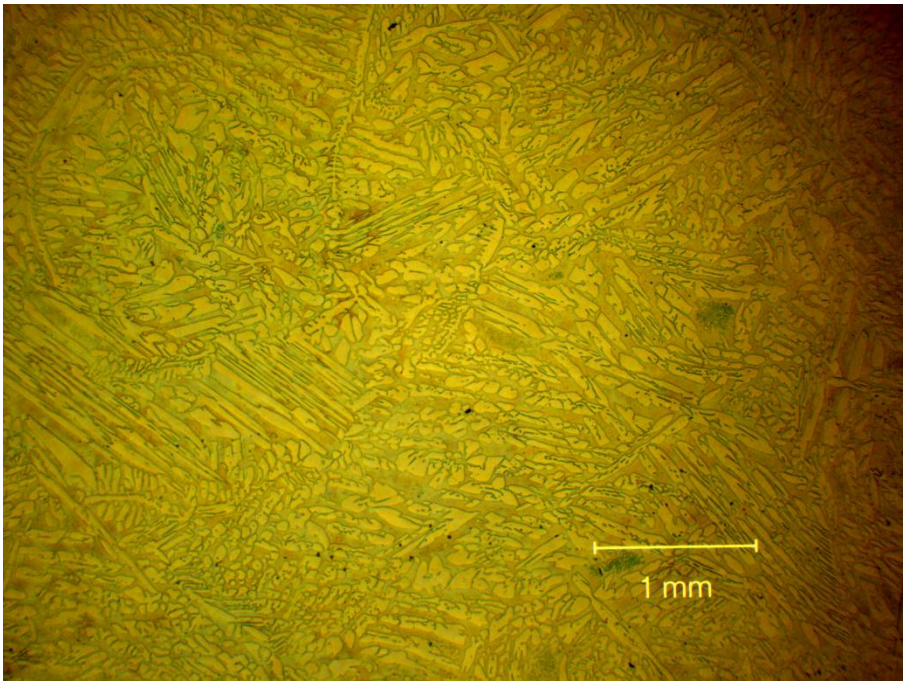

Figure 4.10: Light microscopic image of block 1, reference cast at 1525ºC.

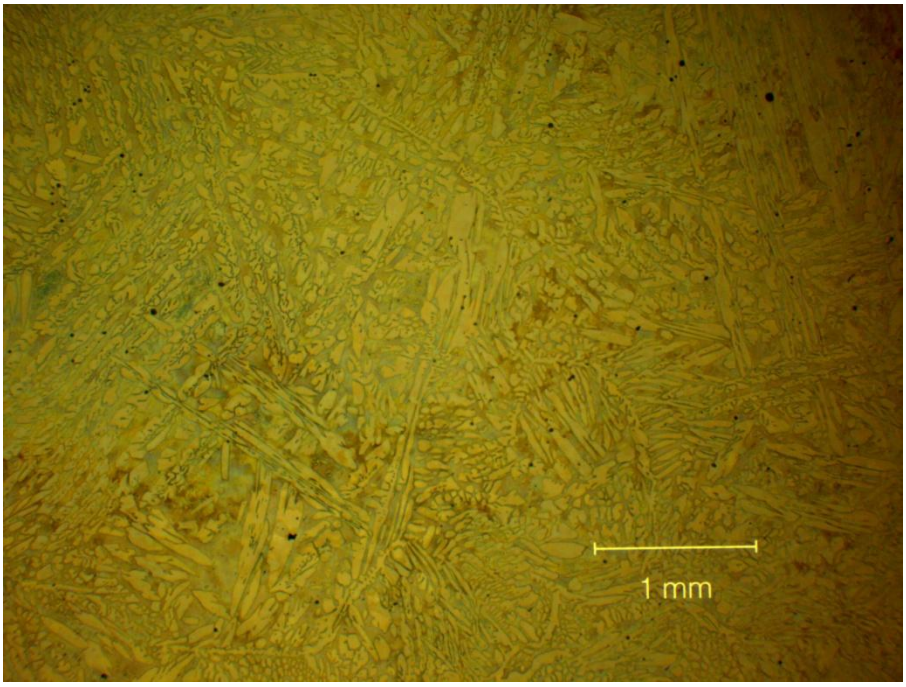

Figure 4.11: Light microscopic image of block 2, 0.034% Ce cast at 1525 ºC.

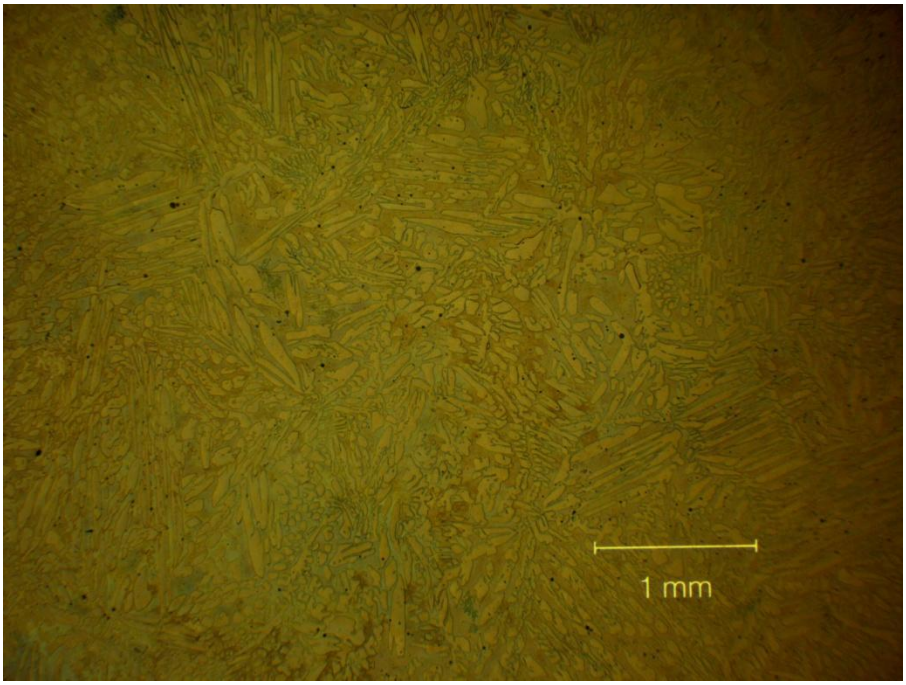

Figure 4.12: Light microscopic image of block 3, 0.036% Ce cast at 1525 ºC.

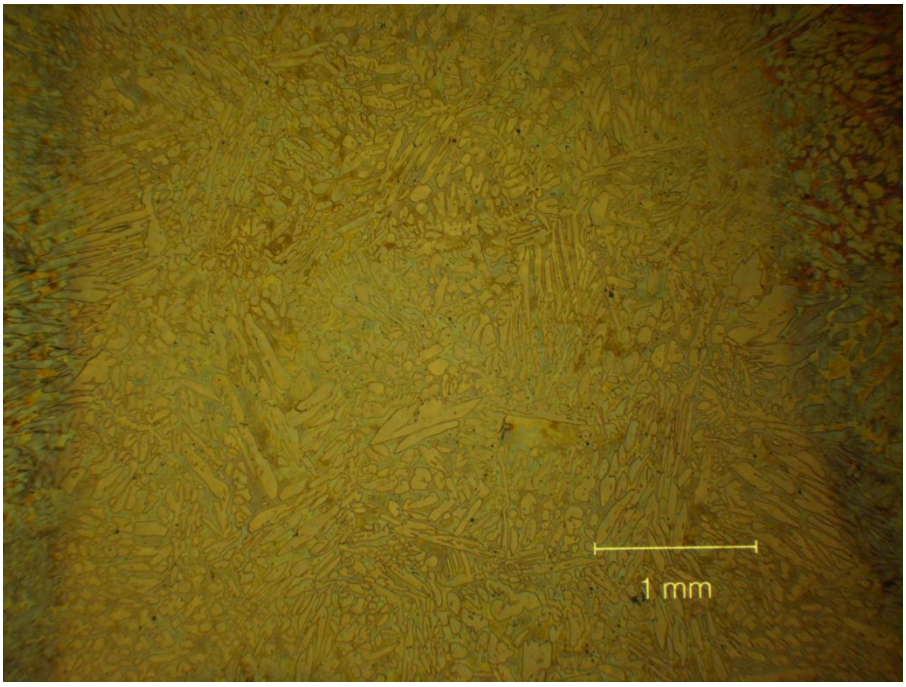

Figure 4.13: Light microscopic image of block 4, 0.064% Ce cast at 1525 ºC.

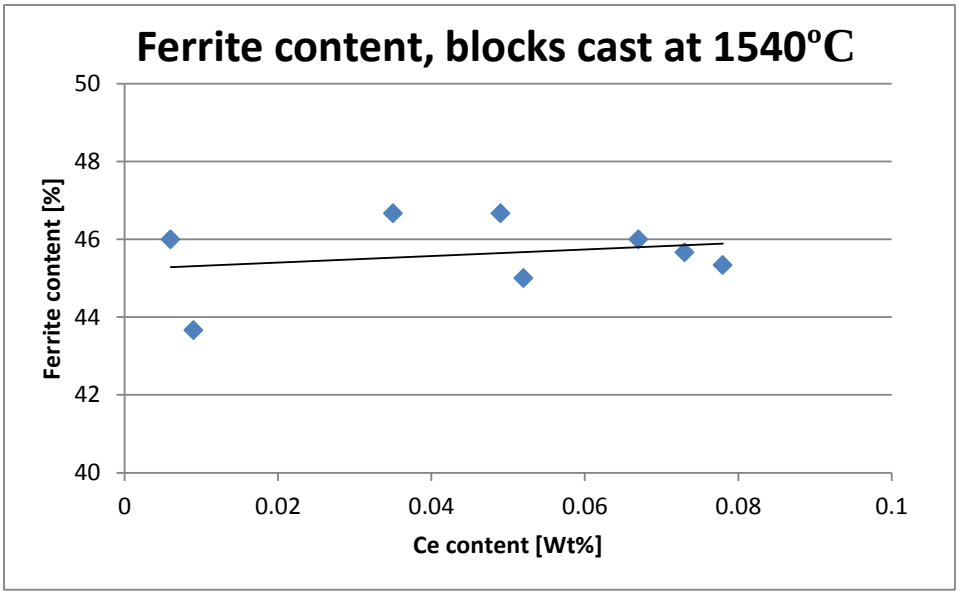

Figure 4.14 Ferrite content versus cerium content for blocks with casting temperature 1540°C.

4.5 EPMA

Figures 4.16-4.26 shows particles analysed with EPMA, some of the particles were analysed quantitatively with the result given in the corresponding table where all values are atomic%. Most of the particles from block with added cerium included 3 different phases; bright, grey and dark, some had only one or two of the phases large enough to analyse. An example from block 8 is shown in figure 4.15 where all three phases are present in the particles. The largest particle in figure 4.18 is also analysed with backscatter electrons in figure 4.24. The blocks without cerium addition had only particles with a single phase.

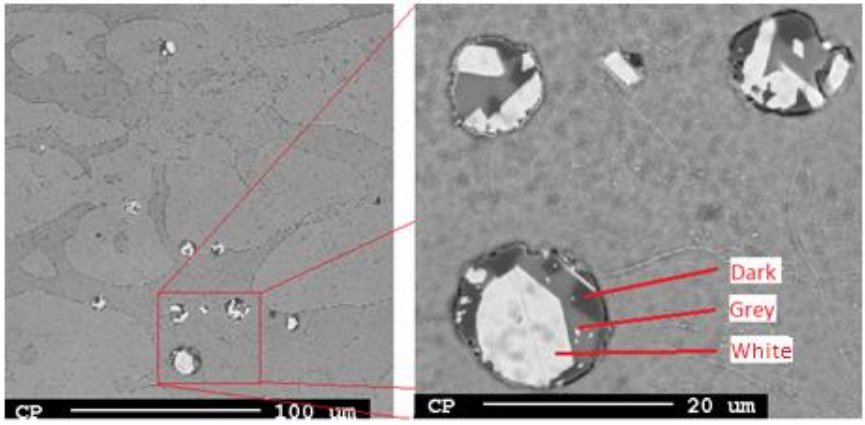

Figure 4.15: Image of particles up close with different contrast, from block 8.

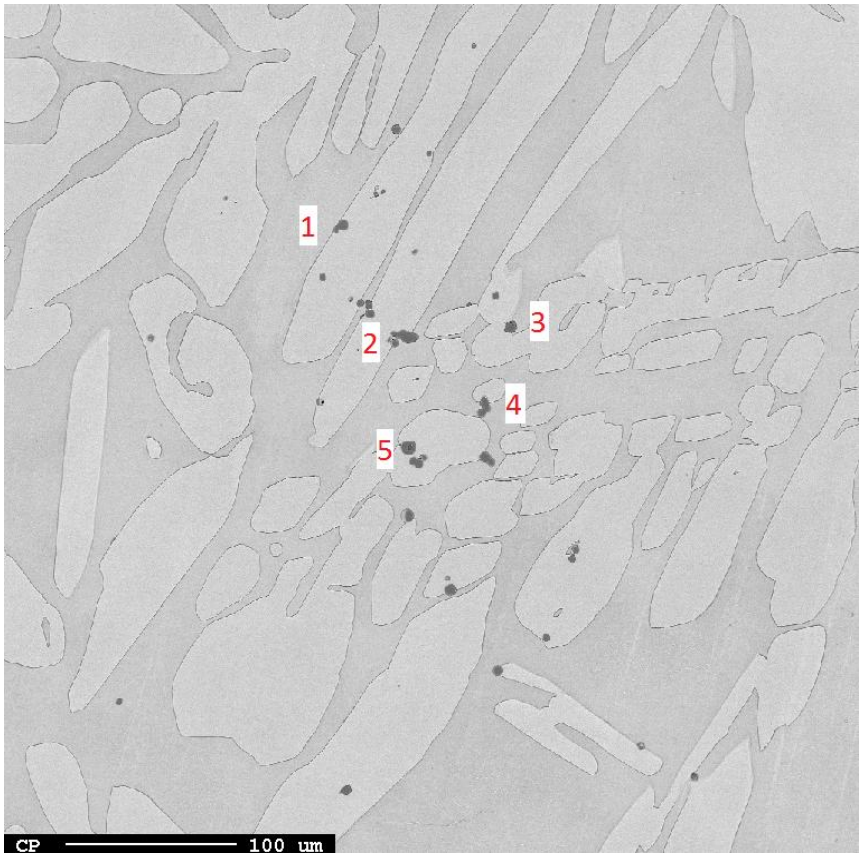

Figure 4.16: Image of particles from block 5 (reference), composition given in table 4.3

Table 4.3: Composition of particles in figure 4.19, and likely phase, all values in atomic%.

#	Al	O	S	C	Cr	Mn	Phase
1	8.3	56.0	0	1.9	19.6	12.7	$(CrMnAl)_2O_3$
2	9.6	56.3	0.1	2.1	17.8	12.7	$(CrMnAl)_2O_3$
3	10.5	56.2	0	2.1	17.2	12.6	$(CrMnAl)_2O_3$
4	10.4	56.3	0	2.1	17. 1	12.5	$(CrMnAl)_2O_3$
5	10.1	56.1	0.1	2.1	17.8	12.5	$(CrMnAl)_2O_3$

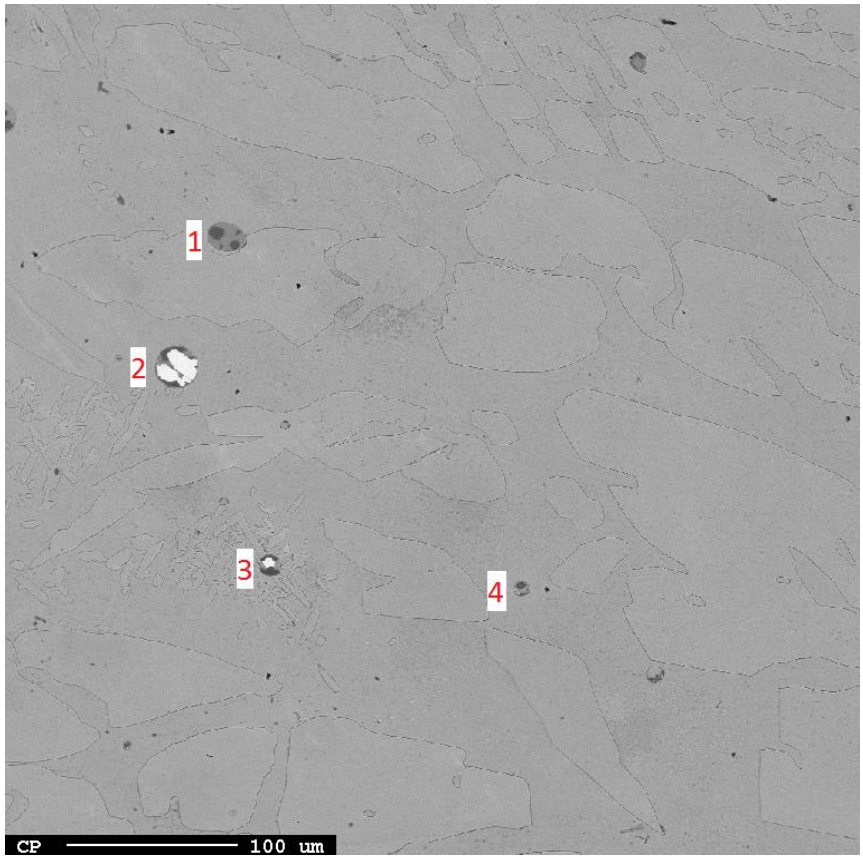

Figure 4.17: Image of particles in block 6 (0.049% Ce), composition given in table 4.4.

Table 4.4: Composition of particles in figure 4.20, and likely phase, all values in atomic%.

#	Area	Al	O	S	C	Cr	Si	Mn	Ce	Phase
1	Grey	7.7	61.3	0	2.4	2.0	14.4	4.1	6.8	$(AlCeSi)_2O_3$
1	Dark	27.7	58.5	0.1	2.7	4.9	0.1	2.1	2.9	AlO_2
2	White	0.3	60.1	0.1	1.9	1.5	13.4	2.2	19.1	$(CeSi)O_2$
2	Grey	8.5	61.3	0.1	3.1	2.7	13.0	4.0	6.1	$(AlCeSi)_2O_3$
2	Dark	11.1	55.0	0	3.0	16.9	0.0	12.6	0.1	$(AlCrMn)_2O_3$
3	White	0.1	58.1	0	1.9	1.2	14.0	3.4	19.4	$(CeSi)O_2$
3	Grey	8.2	61.3	0.1	2.9	1.8	13.4	3.1	8.0	$(AlCeSi)_2O_3$
3	Dark	14.9	55.4	0.1	2.5	13.5	0.1	12.2	0.1	$(AlCrMn)_2O_3$
4	Grey	7.5	61.1	0	3.4	2.2	12.6	3.2	7.4	$(AlCeSi)_2O_3$
4	Dark	10.8	56.6	0	2.8	11.7	3.8	9.2	1.8	$(AlCrMn)_2O_3$

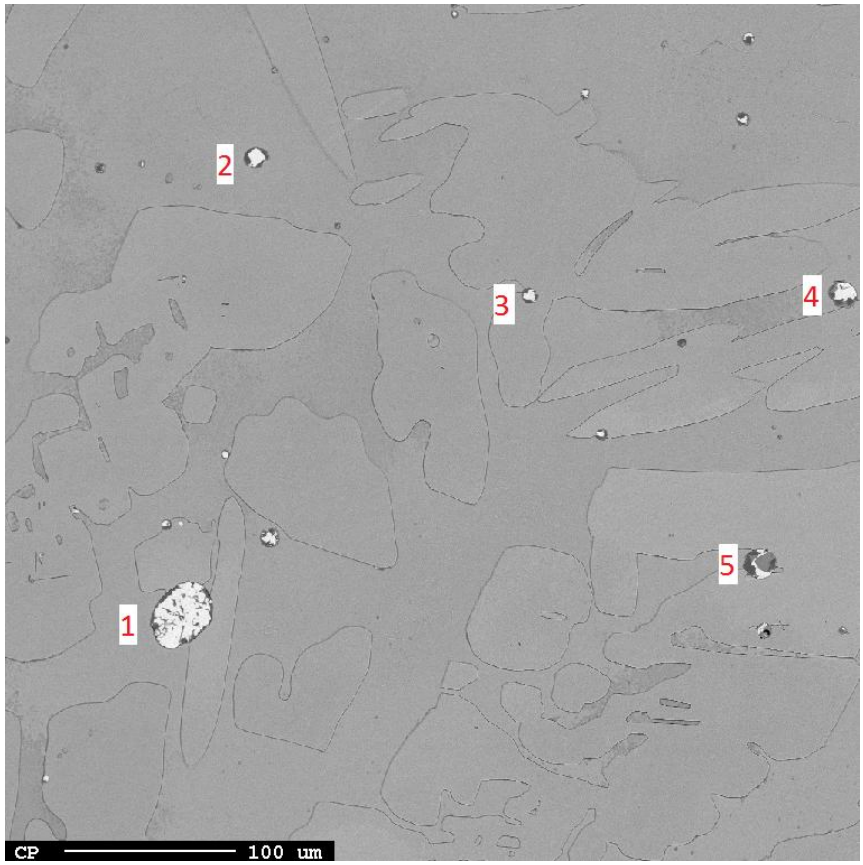

Figure 4.18: Image of particles in block 7 (0.052% Ce), composition given in table 4.5

Table 4.5: Composition of particles in figure 4.21, and likely phase, all values in atomic%.

#	Area	Al	O	S	C	Cr	Si	Mn	Ce	Phase
1	White	0.4	60.2	0	1.3	0.4	13.7	2.0	19.4	$(CeSi)O_2$
2	White	0.0	58.2	0.1	1.6	0.9	14.2	3.3	19.8	$(CeSi)O_2$
2	Dark	29.3	57.8	0.1	2.4	3.9	0.1	2.4	3.1	AlO_2
3	White	0.1	58.3	0	1.5	1.1	14.3	3.5	18.9	$(CeSi)O_2$
3	Dark	14.1	52.8	0.1	2.7	15.4	0.1	11.2	0.5	$(AlCrMn)_2O_3$
4	White	0.1	58.5	0	1.5	1.0	14.1	3.2	19.4	$(CeSi)O_2$
4	Grey	10.5	60.0	0	2.0	2.1	12.9	4.3	6.5	$(AlCeSi)_2O_3$
4	Dark	29.4	57.5	0.1	2.4	4.2	0.1	2.4	3.0	AlO_2
5	White	0.1	58.8	0.1	1.6	1.0	13.8	3.2	18.9	$(CeSi)O_2$
5	Grey	8.7	61.0	0	2.2	2.0	14.2	4.1	6.3	$(AlCeSi)_2O_3$
5	Dark	29.4	57.6	0	2.5	4.1	0.1	2.3	2.9	AlO_2

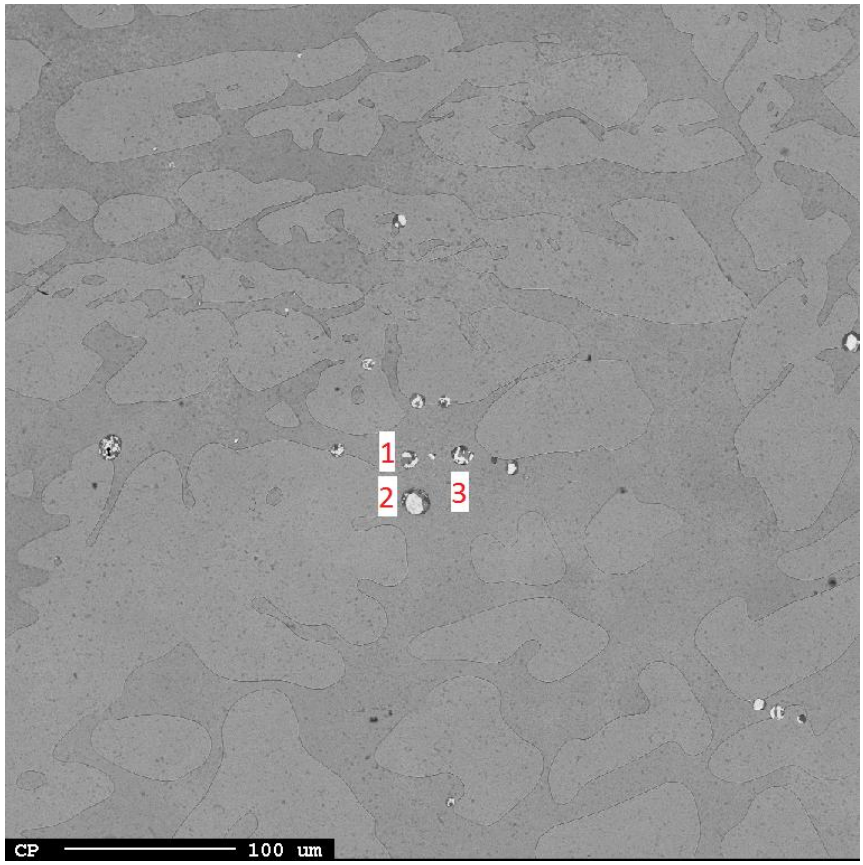

Figure 4.19 Image of particles in block 8 (0.073% Ce), composition given in table 4.6

Table 4.6: Composition of particles in figure 4.22 and likely phase, all values in atomic%.

#	Area	Al	O	S	C	Cr	Si	Mn	Ce	Phase
1	White	0.1	55.4	0	6.0	1.0	13.4	3.3	18.3	$(CeSi)O_2$
1	Grey	8.2	59.1	0	5.5	1.6	13.5	3.9	6.5	$(AlCeSi)_2O_3$
1	Dark	12.0	55.7	0	4.7	11.3	1.2	11.2	2.4	$(AlCrMn)_2O_3$
2	White	0.0	57.8	0.1	7.5	0.7	12.5	2.6	17.0	$(CeSi)O_2$
2	Grey	7.8	58.7	0.1	7.1	1.6	13.4	3.7	6.5	$(AlCeSi)_2O_3$
2	Dark	11.6	56.6	0	5.8	10.0	2.0	11.7	0.5	$(AlCrMn)_2O_3$
3	White	1.2	55.9	0.1	5.6	2.0	8.0	9.7	15.7	$(CeSi)O_2$
3	Grey	7.6	59.7	0	7.3	1.4	12.9	3.7	6.3	$(AlCeSi)_2O_3$
3	Dark	12.8	55.2	0.1	5.8	12.3	0.2	11.8	0.7	$(AlCrMn)_2O_3$

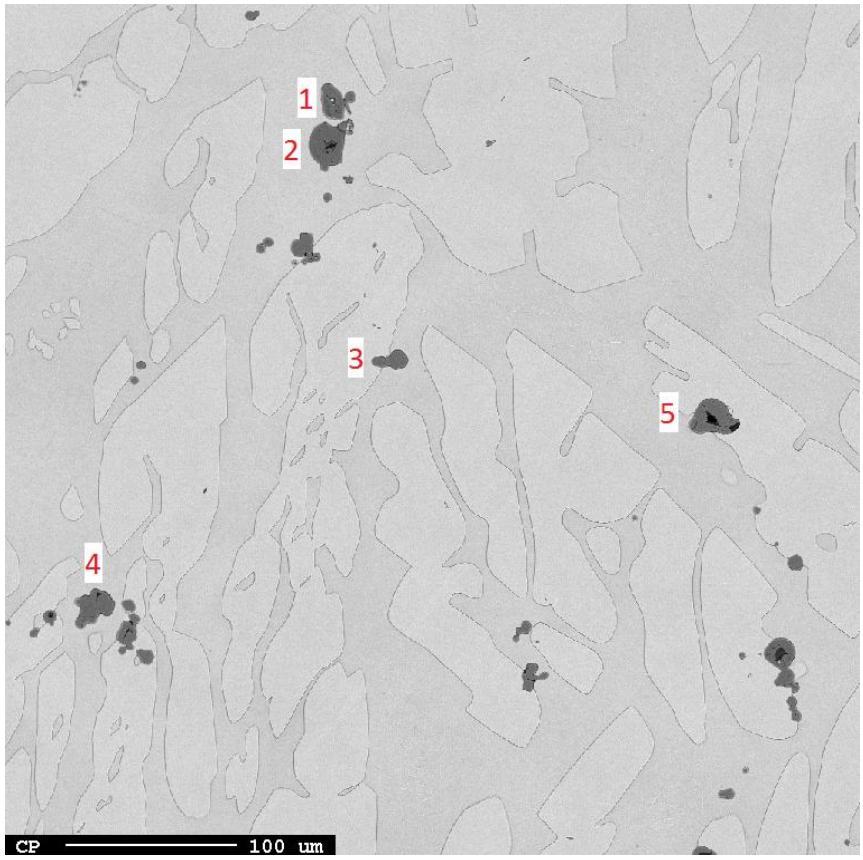

Figure 4.20: Image of particles in block 9 (reference), composition given in table 4.7

Table 4.7: Composition of particles in figure 4.23 and likely phase, all values in atomic%.

#	Al	O	S	C	Cr	Mn	Phase
1	13.5	55.1	0	3.5	14.6	12.4	$(CrMnAl)_2O_3$
2	12.2	54.6	0.1	3.5	15.7	12.4	$(CrMnAl)_2O_3$
3	11.9	54.7	0.1	3.5	16.1	12.4	$(CrMnAl)_2O_3$
4	12.7	54.6	0.1	3.5	15.6	12.5	$(CrMnAl)_2O_3$
5	11.6	54.7	0	3.5	16.6	12.4	$(CrMnAl)_2O_3$

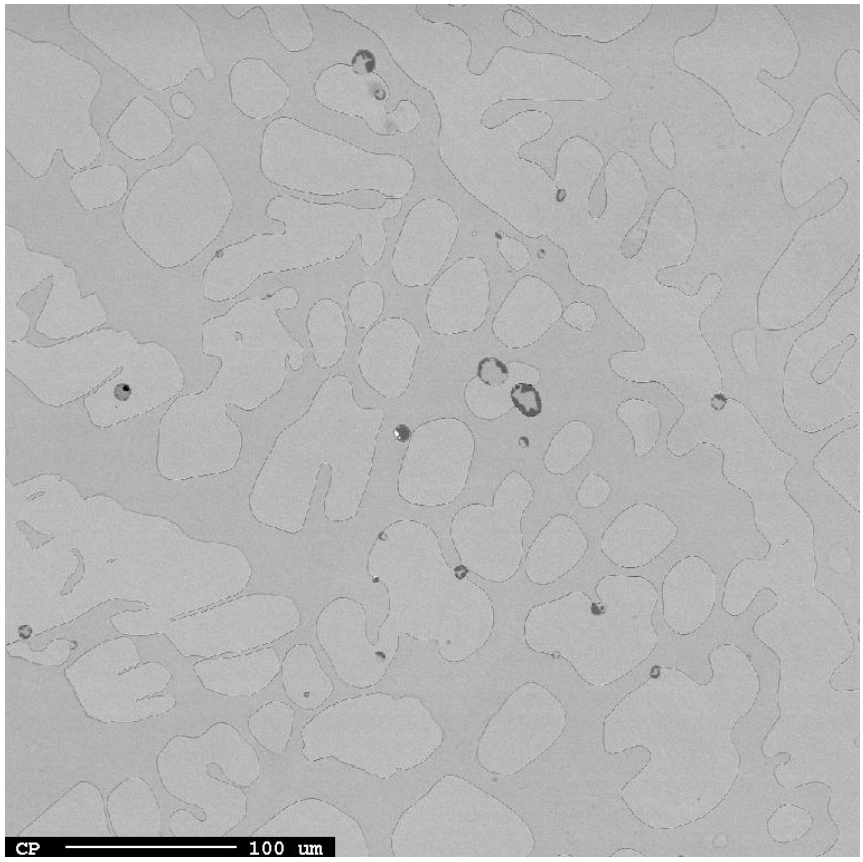

Figure 4.21: Image of block 10 (0.035% Ce) showing little cerium content in found particles.

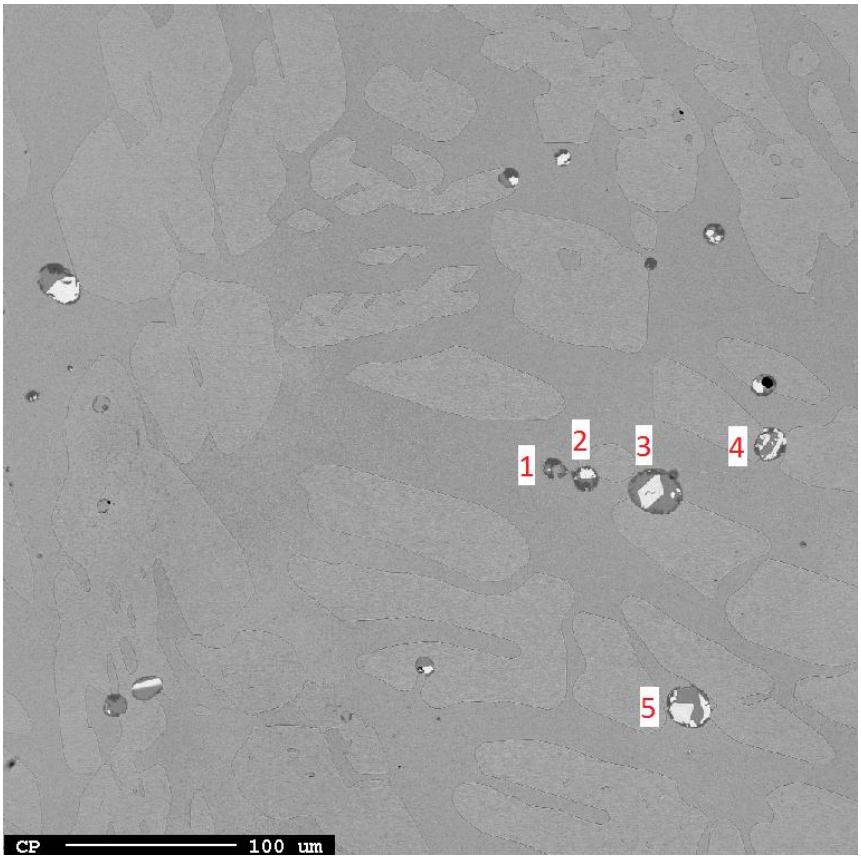

Figure 4.22: Image of block 11 (0.067% Ce), composition given in table 4.7.

Table 4.7: Composition of particles in figure 4.25, and likely phase, all values in atomic%.

#	Area	Al	O	S	C	Cr	Si	Mn	Ce	Phase
1	Grey	7.8	60.2	0.1	4.0	3.2	12.8	4.5	6.0	$(AlCeSi)_2O_3$
1	Dark	11.5	54.8	0.1	3.4	16.4	16.4	12.5	0.1	$(AlCrMn)_2O_3$
2	White	0.2	59.5	0	2.5	1.1	13.0	3.2	18.6	$(CeSi)O_2$
2	Grey	8.2	60.0	0	3.9	2.1	14.0	3.7	6.2	$(AlCeSi)_2O_3$
2	Dark	15.3	55.0	0.1	3.6	13.9	0.1	10.9	0.2	$(AlCrMn)_2O_3$
3	White	0.2	61.5	0	3.7	0.1	15.2	0.2	18.1	$(CeSi)O_2$
3	Grey	7.8	60.9	0.1	3.4	1.9	14.3	4.1	6.6	$(AlCeSi)_2O_3$
4	White	0.1	61.2	0	3.9	0.4	14.9	0.2	17.6	$(CeSi)O_2$
4	Grey	8.0	60.6	0.1	3.8	2.0	14.6	3.9	6.2	$(AlCeSi)_2O_3$
4	Dark	12.1	55.1	0	3.4	15.7	0.1	12.4	0.1	$(AlCrMn)_2O_3$
5	White	0.1	60.5	0	3.4	0.4	14.6	1.4	18.3	$(CeSi)O_2$
5	Grey	7.7	60.5	0.1	4.7	1.8	14.2	3.7	6.4	$(AlCeSi)_2O_3$

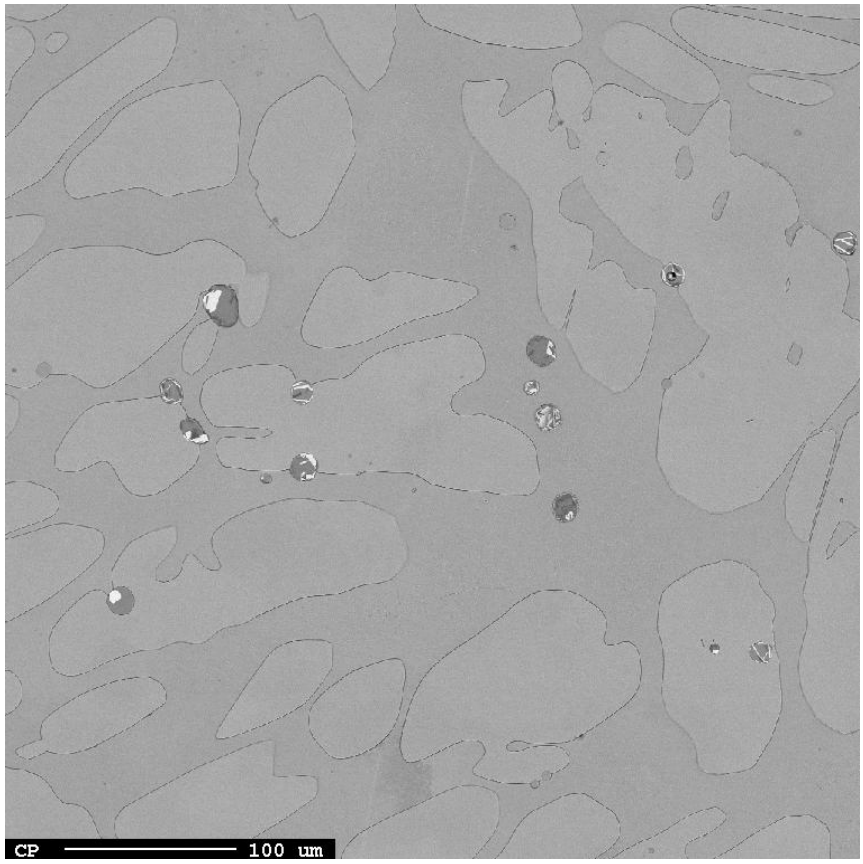

Figure 4.23: Image of particles from block 12 (0.078% Ce), showing particles with different phases.

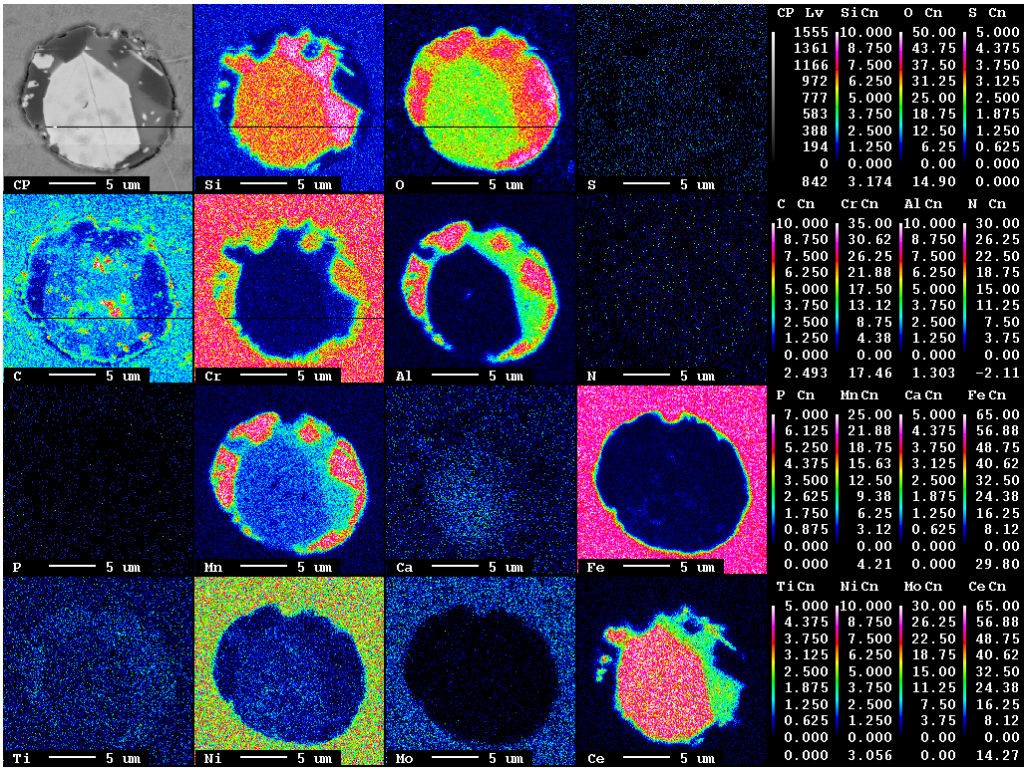

Figure 4.24: Electron backscatter image of particle from block 8, showing all three phases seen in other particles, bright, grey and dark.

4.5 Mechanical testing

The results from the tensile tests are given in figures 4.25-4.27, where the two different cast temperatures is given as green and blue for temperatures 1525ºC and 1540 ºC respectively. Both series show a linear increase in both yield and ultimate tensile strength, the higher cast temperature shows a stronger effect of EGR addition, due to the references is weaker at the higher casting temperature. The series cast at 1540 increases 7.2% and 3.3% in yield and ultimate tensile strength respectively with most Ce added. The lower casting temperature have its peak in ultimate tensile strength with 0.034% Ce (0.075% added) but nearly the same as the block with most cerium. The yield strength result of lower casting temperature is somewhat different from ultimate tensile strength: The results here shows an increase from 533 MPa for the reference to 542 MPa with most cerium (0.064% Ce), while the two

blocks with lower Ce content shows slightly decreased yield compared to the reference. The elongation is increased from 38%, for the reference, to 41% for all three blocks with added cerium. The impact toughness test shows an overall decrease for the blocks with added cerium, from 139 J for the reference to 125 J with 0.036% Ce which was the lowest.

The blocks cast at 1540ºC the elongation does increase a small amount, but the blocks with most cerium have lower elongation than the references. The impact toughness test shows a linear reduction of toughness with increasing cerium content. The lowest value is the block with the lowest cerium content, block 10; 0.035% Ce. However, all results is clearly above the requirements for cast duplex according to the standard. Regarding the reducing of impact toughness which decreases, it is still over 2 times higher than the required energy absorption.

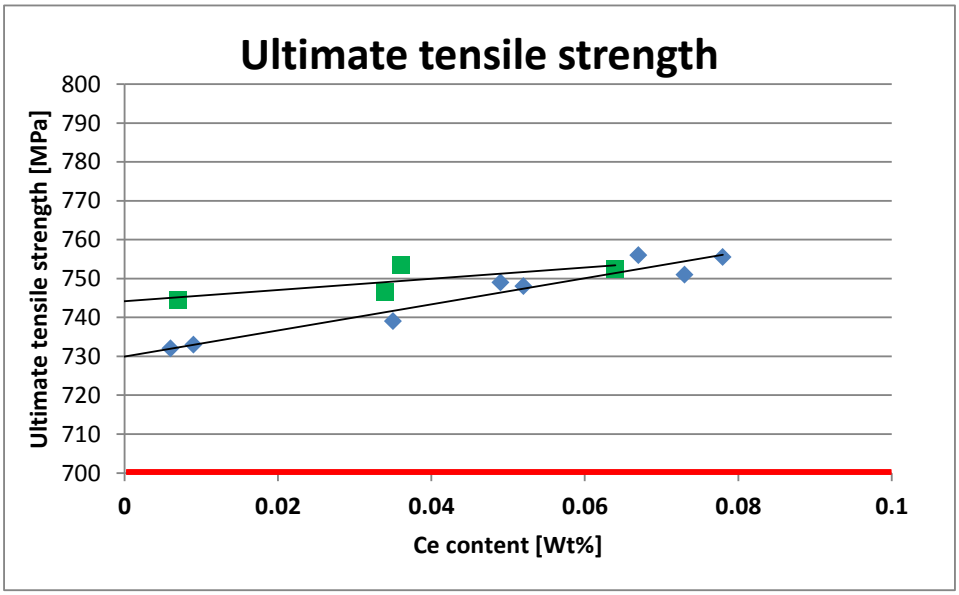

Figure 4.25: Ultimate tensile strength and cerium content, green show series cast at 1525 ºC, blue cast at 1540ºC. Red line show required strength according to standard. [20]

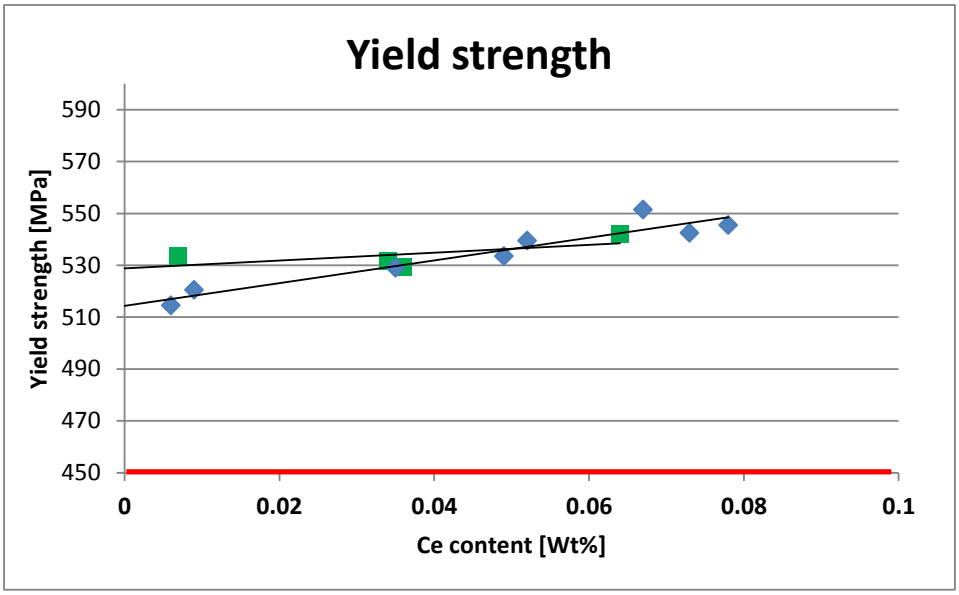

Figure 4.26: Yield strength versus cerium content, green show series cast at 1525 ºC, blue cast at 1540ºC. Red line show required strength according to standard.[20]

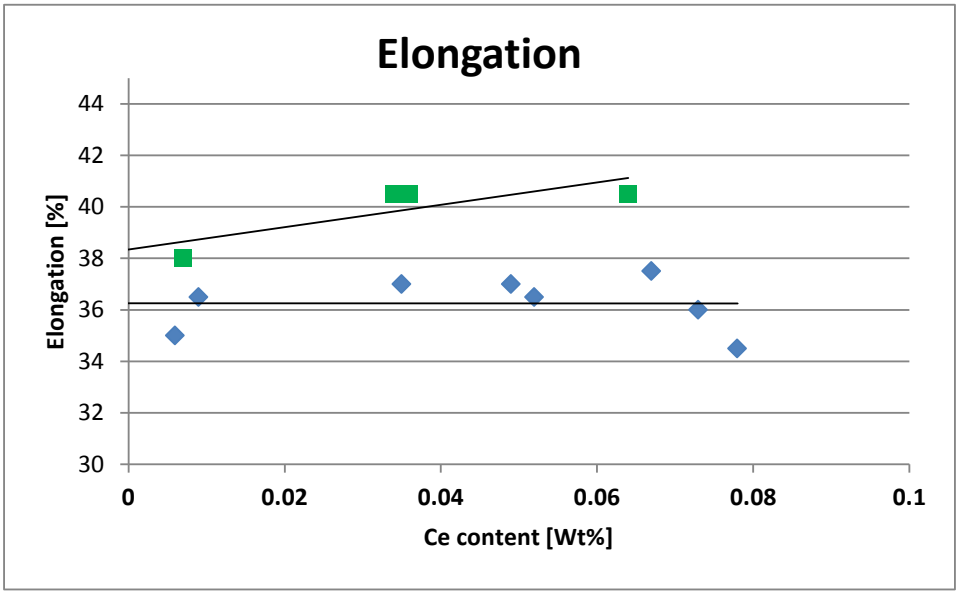

Figure 4.27: Elongation versus cerium content, green show series cast at 1525 ºC, blue cast at 1540ºC. Requirement from standard is 18%.[20]

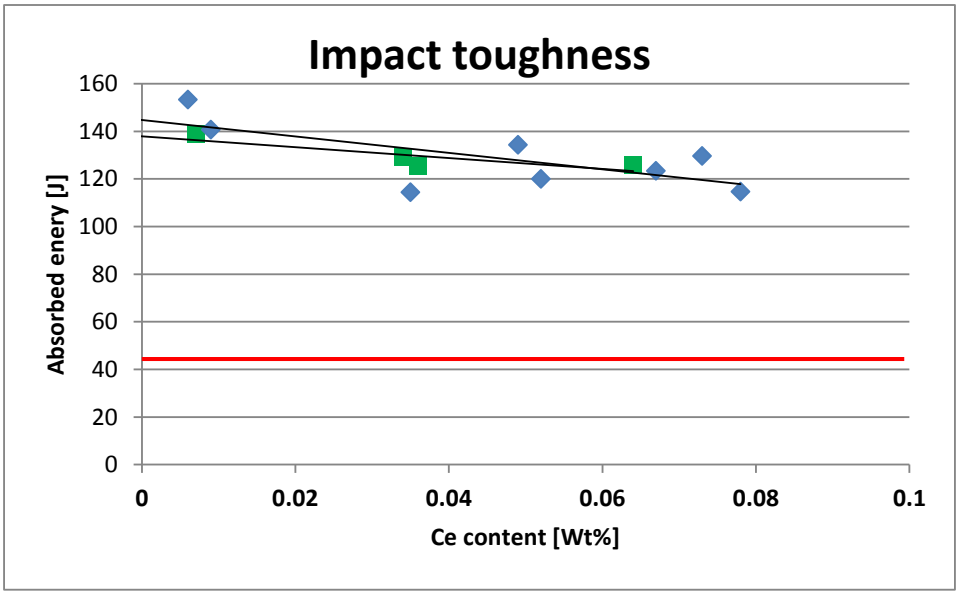

Figure 4.28: Impact toughness at -46 ºC versus cerium content, green show series cast at 1525 ºC, blue cast at 1540ºC. Red line show required strength according to standard.[20]

4.6 SEM

The fracture surfaces from the impact toughness test were examined by EDS in a SEM. Exact composition is not obtained by EDS, but the peaks of graphs give an indication of the amount of elements present. Figures 4.29-4.32 shows a correlation with the composition given in table 4.4. Overall the particle found in the dimples in the fracture surfaces resembles the particles scanned with EPMA, which is mainly cerium-oxide and aluminium-oxides.

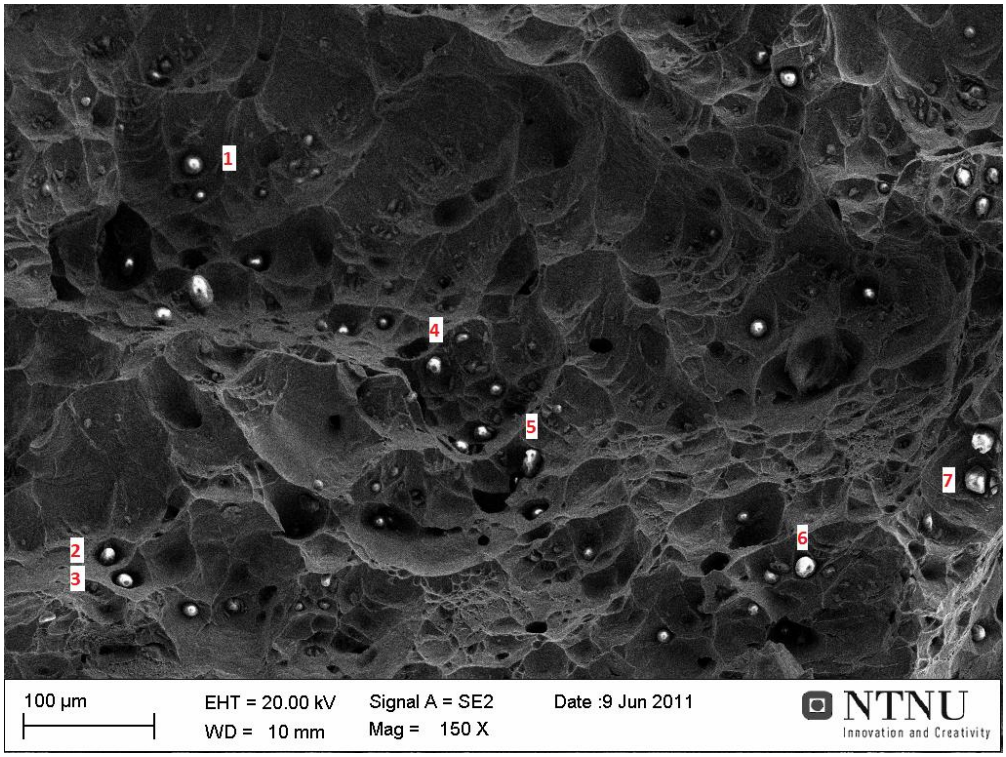

Figure 4.29: Example of EDS scan from block 6, image acquired with secondary electrons, analysis done with backscatter electrons. Numbers indicate particles scanned with results in figures 4.28 – 4.31.

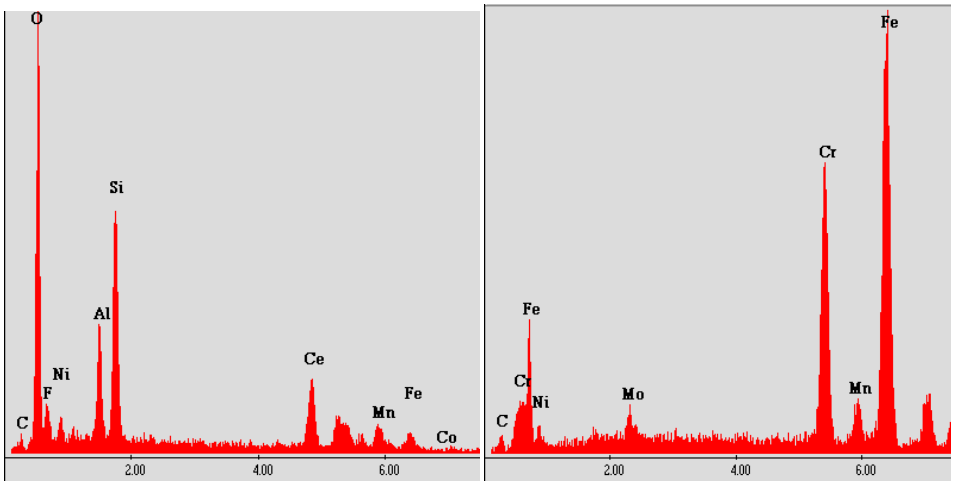

Figure 4.30 (a), (b): EDS scan of particles 1 (a) and 2 (b) from figure 4.28, showing elements present.

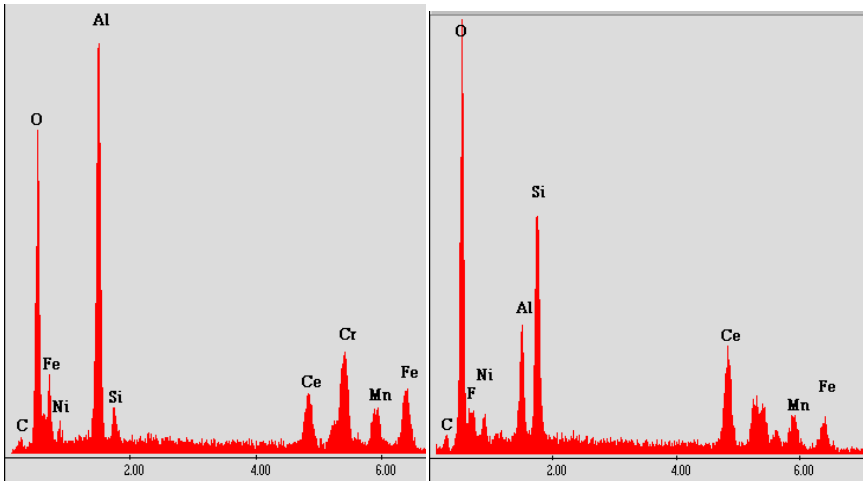

Figure 4.31 (a), (b): EDS scan of particles 3 (a) and 4 (b) from figure 4.28, showing elements present.

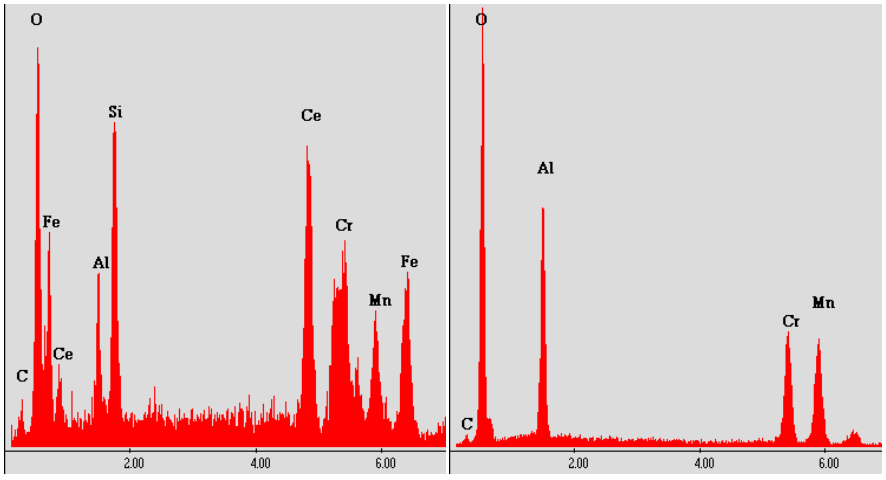

Figure 4.32 (a), (b): EDS scan of particles 5 (a) and 6 (b) from figure 4.28, showing elements present.

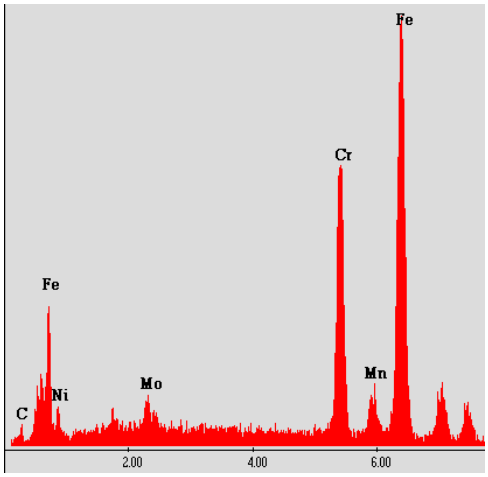

Figure 4.33: EDS scan of particle 7 from figure 4.29, showing elements present.

5. Discussion

5.1 Experiment

The execution of this experiment can influence the results, the yield of cerium added show this. Figure 4.1 shows the relation between added cerium and actual content after casting. The overall yield of 72% is higher than seen in previous trials. The reason for this can be caused by the short time between addition to the ladle and casting trapping particles that would float to the surface if given more time. The large oxygen content is likely to have influenced the yield of cerium, normally the amount of oxygen is lower than the cerium content, but in this case the ratio is nearly 1:1 between cerium and oxygen. The large content of oxygen is partly due to unsuccessful deoxidizing, CaSi was added to the furnace for deoxidizing but this appears to have been insufficient amount, but worked somewhat since no Ca is found in chemical analysis. The chemical analysis found Ce in small amounts in all references; this is likely traces in the ladle after previous cast, or traces from production at Scana since block 1 which was the first to be cast also contains Ce. The holding time of each cast in the ladle was generally short, the time from EGR addition to the ladle was as short as 50 s, which does not give much time for cerium to react and the oxides to distribute through the liquid. As seen from the theory, a holding time of up to 5 minutes is beneficial to the number of inclusions and will give more time for the large inclusions to float to the slag. Mixing of the ladle may be beneficial; inert gas is often used and may help remove the largest inclusions seen in the EPMA analysis.

5.2 As cast structure

The macroscopic examination of the blocks, figure 4.2-4.9, reveals a strong effect of refining the cast structure by adding EGR. The length of the columnar zone was reduced from 22 mm (reference) to 0 for the blocks with the biggest addition of EGR. The grain size of the grains in the equiaxed zone in the middle of the block is also reduced. These results are contributed to the nucleation potential of the cerium particles obtained by adding EGR to the ladle during casting. This in return will affect the segregation of steel, making it more homogeneous and therefore making

the heat treatment more effective in homogenizing the steel. A more homogen steel can contribute to the increased mechanical properties of the blocks with 0.075% Ce added; the macro etch reveals a columnar zone present but the mechanical tests show almost as good results as the blocks which does not have a columnar zone present at all.

5.3 Light microscopic examination

The light microscopic examination is somewhat insufficient, due to the lack of quantifying the grain size. It is a difficult task because of the dual phase composition of the steel. It was suggested that the best technique for determining a grain size is using EBSD, where each grain will get different colour due to lattice rotation. The ferrite amount was measured with light microscope and software at Scana steel. The result is given in appendix 2, but does not seem to vary significantly with cerium content.

5.4 Cerium particles in the metal

The particles found and identified by EPMA examination fits with the theory of the strong oxidizing effect of cerium. The type of particles does not seem to vary with larger Ce addition. Almost all particles found with cerium content also consist of phases without cerium, while the particles found in the references contained only a single phase. The particles analysed did not contain any sulphur which is the most beneficial cerium inclusion regarding undercooling and lattice misfit.

5.5 Mechanical tests

The tensile tests show a linear increase in strength for increased cerium content; this is contributed to the refined casting structure. The mechanical test also show a decreasing impact toughness, this effect are most likely due to the increased particle content, which also correlates to the theory [15]. The results show different effect of EGR to elongation; for the series cast at 1525ºC the elongation increases. The series cast 1540ºC the elongation is increasing except for the 2 blocks with the largest EGR addition, which causes this series to show no influence to the elongation overall.

The casting temperature does not seem to affect the mechanical properties of the grain refined blocks. The reference for the series cast at 1525°C is

stronger than its counterpart cast at 1540°C making the increased mechanical properties obtained by adding EGR smaller for the lower casting temperature. The only mechanical difference between the series is elongation, where blocks cast at 1525°C shows a linear increase with increased Ce content, while blocks cast at 1540°C show no overall effect on elongation.

During machining blocks 3 and 4 were accidentally cut the wrong way, causing the tensile bars from these blocks to be cut lower in the block. This deviation is not considered to have influenced the result significantly since figure 4.2 and 4.3 shows the same trend as for the series cast at 1540ºC, figure 4.6 and 4.7. From block 6 one of the tensile bars was label "abnormal" from the test lab, resulting in too high ultimate tensile strength. If this bar is included; figure 4.6 will look like figure 5.1, which shows the abnormal bars influence on the graph and does not follow the linear trend in figure 4.6.

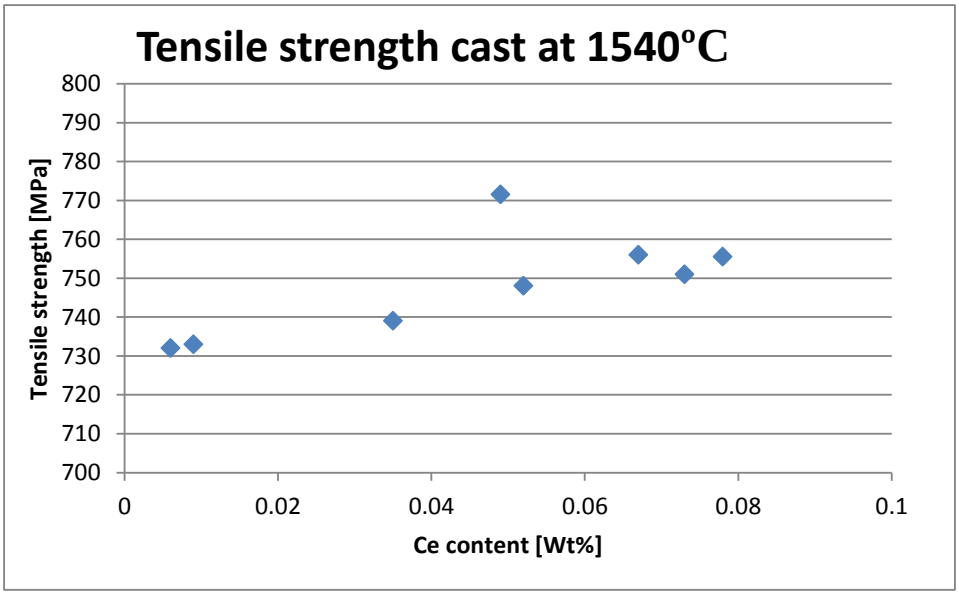

Figure 5.1: Ultimate tensile strength versus cerium content, with included abnormal specimen.

5.6 Effect of casting temperature

The two different casting temperatures used in this experiment does not seem to affect EGR's potential for grain refining. Neither the as cast structure, mechanical properties or particles present varies significantly with change of casting temperature. The only notable difference between the 2 series were increased strength in reference cast at 1525°C compared to the references cast at 1540°C.

Mikrostrukturen..
Tid brukt på støpinga, boble argon
Fraværet av svovel

6. Conclusion

The conclusions based on this work are the following:

By adding EGR to liquid Super Duplex steel it will react with available oxygen to form complex particles containing $(CeSi)O_2$, $(AlCeSi)_2O_3$, $(AlCrMn)_2O_3$

With the correct amount of EGR added to Super Duplex the as cast structure is greatly refined, ultimately eliminating the columnar zone completely.

The refining of Super Duplex with EGR can result in an increase of 7% and 3% for yield and ultimate tensile strength respectively.

Reducing the cast temperature from 1540 to 1525 for Super Duplex steel has no effect of EGRs potential for grain refining.

Proposal for further work

From the positive results in this experiment by adding EGR to Super Duplex steel, there is possible to enhance the mechanical properties considerably. The large oxygen content in the steel is likely to be reduced by performing the casting by refining in an AOD converter where process control is better. Also an experiment where the holding time is controlled may be beneficial to explore optimal conditions for grain refining with EGR.

References

1. Gunn, R., *Duplex Stainless Steels*. 1997: Abington Publishing.
2. Flemings, M.C., *Solidification Processing*. 1974: McGraw Hill Inc.
3. Porter, D.A., K.E. Easterling, and M.Y. Sherif, *Phase Transformations in Metals and Alloys*. 2009: CRC Press.
4. Nilsson, M.R., *Kornförfining av stål, del 2*. 2007, Swecast.
5. Lidegran, P., *Microprobe investigation of A17061 sample received from Siepmann*. 2008.
6. Verhoeven, J.D., *Fundamentals of Physical Metallurgy*. 1975: John Wiley & Sons, Inc.
7. Dieter, G.E., *Mechanical Metallurgy*. 1988: McGraw-Hill Book Company.
8. Engh, T.A., *Principals of Metal Refining*. 1992: Oxford Science Publications.
9. Akselsen, O.M., C.v.d. Eijk, and Ø. Grong, *Grain refinement of steel castings*, O.M. Akselsen, Editor. 1999, SINTEF.
10. MuxingGUO and H. SUITO, *Influence of Dissolved Cerium and Primary Inclusion Particles Ce203 and CeS on Solidification Behavior of Fe-0.20 mass% C-0.02 mass%PAlloy.* ISIJ International, 1999. **39**(7): p. 722-729.
11. Haakonsen, F., *Optimizing of Strømhard austenitic manganese steel.*, in *Material Science and Engineering*. 2009, Norwegian University of Science and Technology.
12. Dahle, E.S., *EGR additions to austenitic manganese steel.* SINTEF F18030, 2011.
13. Eijk, C.v.d., et al., *Grain Refinement of Fully Austenitic Stainless Steels Using a Fe-Cr-Si-Ce Master Alloy*, in *59th Electric Furnace and 19th Process Technology Conferences,*. 2001: Phoenix, AZ USA.
14. Eijk, C.v.d. and A. Slettan, *NYKURS-Project: Grain Refinement of Stainless Steels by Ce Additions.* STF24 F01215, 2001.
15. Thornton, P.A., *The Influence of Nonmetallic Inclusions on the Mechanical Properties of Steel: A Review.* Journal of Material Science, 1971. **6**: p. 347-356.
16. Guo, M. and H. Suito, *Dispersion of Primary inclusions of Ce2O3 and CeS in Fe-O.20 mass% C-0.02 mass%P Alloy.* ISIJ International, 1999. **397**(7): p. 678-686.

17. Blair, M., *Cast Stainless Steels, Properties and Selection: Irons, Steels, and High-Performance Alloys*. ASM Handbook. Vol. 1. 1990: ASM International.
18. Solberg, J.K., *Teknologiske metaller og legeringer*. 2009: Tapir.
19. Park, Y.-H. and Z.-H. Lee, *The effect of nitrogen and heat treatment on the microstructure and tensile properties of 25Cr–7Ni–1.5Mo–3W–xN duplex stainless steel castings.* Material Science And Engineer, 2001. **A297**: p. 78-84.
20. Norsok, *Material data sheets for piping M630*. 2004.

Appendix

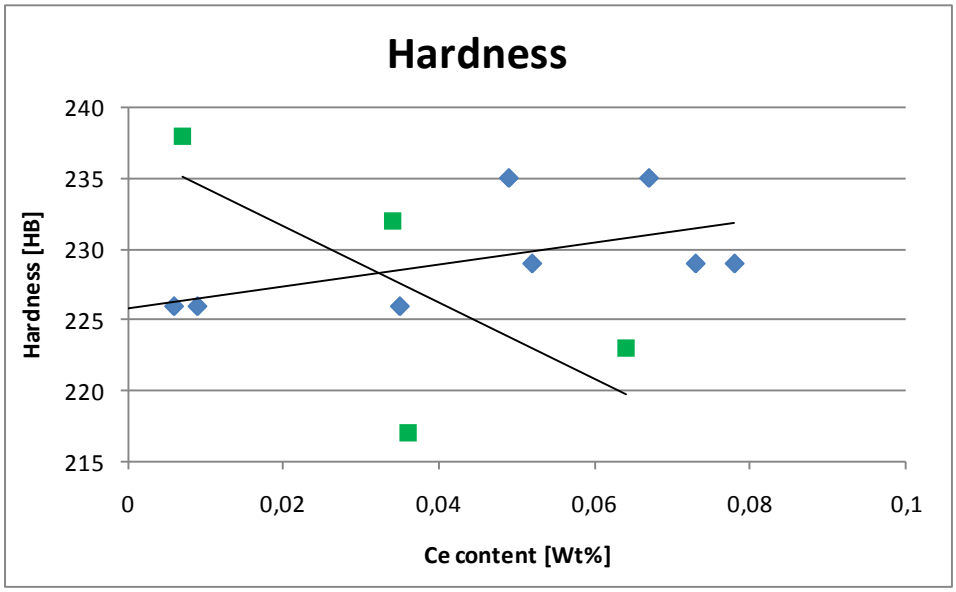

Figure: Hardness versus Ce content.